FINAL REPORT

COMPACT 4-D OPTICAL NEURAL NETWORK ARCHITECTURE

Prepared for

USAF, AFSC
Air Force Office of Scientific Research
Building 410
Bolling Air Force Base, DC 20332-6448

Contract No. F49620-89-C-0120, Project No. 3005/A1

"The views and conclusions contained in this document are those of the authors and should not be interpreted as necessarily representing the official policies or endorsements, either expressed or implied, of the Air Force Office of Scientific Research or the U.S. Government."

By

Philip D. Henshaw, Steven A. Lis, and Norman R. Guivens, Jr.

25 April 1990

SPARTA, Inc.
24 Hartwell Avenue
Lexington, MA 02173
(617) 863-1060

UNCLASSIFIED
SECURITY CLASSIFICATION OF THIS PAGE

REPORT DOCUMENTATION PAGE

1a. REPORT SECURITY CLASSIFICATION UNCLASSIFIED	1b. RESTRICTIVE MARKINGS
2a. SECURITY CLASSIFICATION AUTHORITY	3. DISTRIBUTION/AVAILABILITY OF REPORT Approved for public release; distribution unlimited.
2b. DECLASSIFICATION/DOWNGRADING SCHEDULE	
4. PERFORMING ORGANIZATION REPORT NUMBER(S) LTR90-006	5. MONITORING ORGANIZATION REPORT NUMBER(S) AFOSR-TR- 90-0530
6a. NAME OF PERFORMING ORGANIZATION SPARTA INC. — 6b. OFFICE SYMBOL (If applicable)	7a. NAME OF MONITORING ORGANIZATION Same as 8a
6c. ADDRESS (City, State, and ZIP Code) 24 HARTWELL AVENUE LEXINGTON, MA 02173	7b. ADDRESS (City, State, and ZIP Code) Same as 8c
8a. NAME OF FUNDING/SPONSORING ORGANIZATION AF OFFICE OF SCIENTIFIC RES. — 8b. OFFICE SYMBOL (If applicable) NE	9. PROCUREMENT INSTRUMENT IDENTIFICATION NUMBER F49620-89-C-0120
8c. ADDRESS (City, State, and ZIP Code) USAF, AFSC BLDG 410 BOLLING AIR FORCE BASE, DC 20332-6448	10. SOURCE OF FUNDING NUMBERS PROGRAM ELEMENT NO. 61102F — PROJECT NO. 3005/A1 — TASK NO. — WORK UNIT ACCESSION NO.
11. TITLE (Include Security Classification) COMPACT 4D OPTICAL NEURAL NETWORK ARCHITECTURE	
12. PERSONAL AUTHOR(S) PHILIP D. HENSHAW, STEVEN A. LIS, NORMAN R. GUIVENS, JR.	
13a. TYPE OF REPORT FINAL REPORT — 13b. TIME COVERED FROM 8/15/89 TO 4/15/90 — 14. DATE OF REPORT (Year, Month, Day) 4/25/90 — 15. PAGE COUNT 74	
16. SUPPLEMENTARY NOTATION	

17. COSATI CODES			18. SUBJECT TERMS (Continue on reverse if necessary and identify by block number)
FIELD	GROUP	SUB-GROUP	4D INTERCONNECT SPATIAL LIGHT MODULATOR NEURAL NETWORK

19. ABSTRACT (Continue on reverse if necessary and identify by block number)

This Final Report describes the results of a Phase I SBIR project to investigate 4D optical interconnects recorded in inhomogeneously broadened absorbers.

Our concept has the potential to provide much larger numbers of interconnects than can be achieved using electronics. The need for an extremely large number of interconnects was considered in a recent DARPA-sponsored study.[1] There are a number of applications which might require more interconnections than can be realized using electronics (about equal to a dumb honeybee). For example, vision applications, including infrared search and track, may require more than 10^{10} interconnects and 10^{13} interconnects per second.

Our interconnect architecture makes use of holographic interconnects stored in spectral hole burning (SHB) materials. The use of holography provides access to a volume of material to achieve a very large storage capacity of interconnect values.

20. DISTRIBUTION/AVAILABILITY OF ABSTRACT ☒ UNCLASSIFIED/UNLIMITED ☐ SAME AS RPT. ☐ DTIC USERS	21. ABSTRACT SECURITY CLASSIFICATION UNCLASSIFIED
22a. NAME OF RESPONSIBLE INDIVIDUAL Craig	22b. TELEPHONE (Include Area Code) 202-767-4931 — 22c. OFFICE SYMBOL NE

DD FORM 1473, 84 MAR — 83 APR edition may be used until exhausted. All other editions are obsolete.

SECURITY CLASSIFICATION OF THIS PAGE

19. ABSTRACT (cont.)

The work described here makes use of presently available materials in new ways. Our 4D concept is based on the unique properties of spectral hole burning materials. In addition to the three spatial dimensions available using volume holographic techniques, a fourth, independent dimension, laser frequency is available. This independent dimension is achieved by using materials capable of recording information at one specific laser wavelength which cannot be seen by any other wavelength. By making use of additional laser wavelengths, information can be stored and read independently at many laser wavelengths. In this report we also discuss a second recording mechanism using index of refraction changes which has important advantages for the available spectral hole burning materials.

Our 4D interconnect concept provides a way to fold the access to the four spectral and spatial dimensions into a compact package. The use of four independent dimensions allows implementation of a completely general 2D to 2D interconnect. This general 2D to 2D interconnection capability makes optimum use of the space-bandwidth product of the spatial light modulators used to supply the input and training patterns.

All of the known spectral hole burning materials operate at cryogenic temperature. (4K). The use of cryogenic materials in this application is not a serious drawback because refrigerators are available which are compact and which have low power consumption. For example, APD Cryogenics makes a closed-cycle refrigeration system which can provide at least 1 W of cooling at 4.2 K.[2] This system has sufficient cooling capacity to cool a large number (100 or more) of interconnect modules. This overcapacity means that the size and weight (200 Kg) of this system could be reduced considerably for applications requiring a small number of interconnects.

TABLE OF CONTENTS

1 Introduction

This Final Report describes the results of a Phase I SBIR project to investigate 4D optical interconnects recorded in inhomogeneously broadened absorbers.

Our concept has the potential to provide much larger numbers of interconnects than can be achieved using electronics. The need for an extremely large number of interconnects was considered in a recent DARPA-sponsored study.[1] There are a number of applications which might require more interconnections than can be realized using electronics (about equal to a dumb honeybee). For example, vision applications, including infrared search and track, may require more than 10^{10} interconnects and 10^{13} interconnects per second.

Our interconnect architecture makes use of holographic interconnects stored in spectral hole burning (SHB) materials. The use of holography provides access to a volume of material to achieve a very large storage capacity of interconnect values.

The work described here makes use of presently available materials in new ways. Our 4D concept is based on the unique properties of spectral hole burning materials. In addition to the three spatial dimensions available using volume holographic techniques, a fourth, independent dimension, laser frequency is available. This independent dimension is achieved by using materials capable of recording information at one specific laser wavelength which cannot be seen by any other wavelength. By making use of additional laser wavelengths, information can be stored and read independently at many laser wavelengths. In this report we also discuss a second recording mechanism using index of refraction changes which has important advantages for the available spectral hole burning materials.

Our 4D interconnect concept provides a way to fold the access to the four spectral and spatial dimensions into a compact package. The use of four independent dimensions allows implementation of a completely general 2D to 2D interconnect. This general 2D to 2D interconnection capability makes optimum use of the space-bandwidth product of the spatial light modulators used to supply the input and training patterns.

All of the known spectral hole burning materials operate at cryogenic temperature. (4K). The use of cryogenic materials in this application is not a serious drawback because refrigerators are available which are compact and which have low power consumption. For example, APD Cryogenics makes a closed-cycle refrigeration system which can provide at least 1 W of cooling at 4.2 K.[2] This system has sufficient cooling capacity to cool a large number (100 or more) of interconnect modules. This overcapacity means that the size and weight (200 Kg) of this system could be reduced considerably for applications requiring a small number of interconnects.

1.1 Organization of This Report

Section 2 provides the motivation, answering such key questions as: Why do we want very large networks? What are the limitations of existing concepts? What is our concept and why can it overcome these problems?

Our goal in Phase I was to characterize the properties of a 4D optical interconnect neural network "building block" based on current and projected properties of spectral hole burning media. The Phase I Statement of Work contained five major tasks:

1. Perform an analysis of spectral hole burning materials and project potential performance for 4D interconnect applications.

2. Determine the architecture requirements for (a) writing connections, (b) using connections, (c) learning, and (d) refreshing connection values. Estimate near-term and far-term building block performance. Identify key issues which must be addressed if far-term performance is to be reached.
3. Determine spatial light modulator requirements for a 4D interconnect device.
4. Define a set of experiments to address the key issues determined in items 1, 2, and 3.
5. Prepare a Final Report describing the results of Phase I.

The results of the four technical tasks of our Phase I Statement of Work are presented in this report. Section 3 reports our analysis of burning frequency channels in SHB media. We show that it should be possible to create frequency channels with sharp edges. These sharp edges will allow modulation of the refractive index on the highly transmitting side of the channel edge by changing the absorption on the highly absorbing side of the band edge. Recording highly efficient phase holograms in SHB media should be possible using this technique. In Section 4 we describe our neural network architecture, which makes use of optical interconnects and electronic non-linearity and feedback in a natural way. The component requirements for the optics, laser, detector, and recording material are analyzed in this section. The requirements for the spatial light modulator, one of the key system components, are closely linked to the choices of the other system components. These SLM requirements are summarized in Section 5. The fourth Statement of Work task, defining a set of experiments for Phase II, is reported in Section 6 of this report.

2 Motivation for the 4D Interconnect Concept

Our system can potentially implement extremely large networks. In this section, we will motivate further development of our concept by addressing several key questions: Why do we want very large networks? What are the limitations of existing concepts? What is our concept and why can it overcome these problems?

2.1 Requirements for Neural Network Size

Optics and electronics are competitors for implementation of neural networks. Electronics has the advantages of being a mature technology, of coupling well to existing computers, and of energy efficient computation, required for thresholding at each neuron. Optics has advantages in the interconnect area; although reasonable number of interconnects can be implemented electronically, many more optical communication channels can use the same medium simultaneously. The advantages of optics become important when extremely large numbers of interconnections are required.

Are extremely large numbers of interconnects really required? This question was considered in a recent DARPA-sponsored study.[3] Figure 1 shows a result of the study group's consideration of the connectivity of various biological organisms. Each organism is characterized by the estimated total number of connections between neurons and the number of connections used per second. The study also estimated the future capabilities of electronic and optical implementations of networks; these are shown in Figure 2 on the same axes, interconnects and interconnects per second. We have added the projected capabilities of a 4D interconnect device connecting two fully-populated 1000×1000 element planes and operating at a frame rate of 1 KHz.

Applications for artificial neural networks include robotic control, speech understanding, signal processing, and vision. The requirements for these applications vary widely. Robotic control requirements have been estimated to be between 10^2 and 10^4 interconnects and interconnects per second, while other applications may have far more stressing requirements. For example, vision applications, including infrared search and track, may require more than 10^{10} interconnects and 10^{13} interconnects per second. Weather prediction, not discussed in the DARPA report, may have requirements far exceeding even those of vision.[4] Figure 3 summarizes the requirements, in terms of interconnects and interconnects/sec, for a number of potential applications. Clearly, as more powerful neural network realizations become available, important new applications will appear. One of the goals of our Phase II work will be to identify some of these applications and design a demonstration to show this applicability.

We conclude from these estimates that implementing hardware capable of being trained to be as smart as a honeybee is at the limit of what electronics can provide. Surpassing this capability should be possible through the use of optics. In the remainder of this section, we will present reasons why our 4D interconnect concept can surpass other optical implementations. In Section 5.2 we will present results of our Phase I architecture study showing how our 4D interconnect concept can be used in a neural network processor.

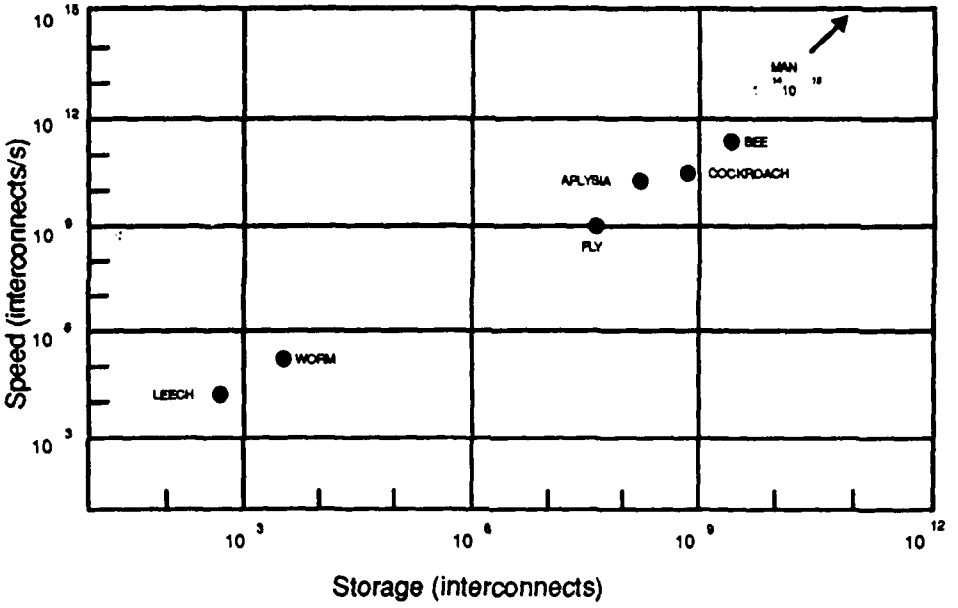

Figure 1. Estimated connectivity of various biological organisms. (Adapted from DARPA Neural Network Study Final Report, 1988.)

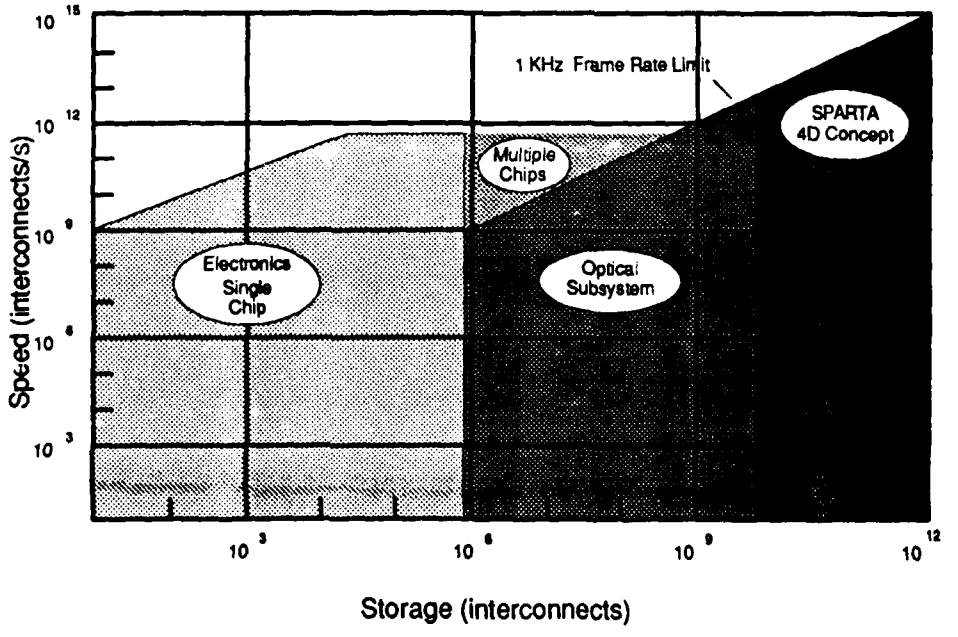

Figure 2. Projected capabilities of electronic and optical implementations of networks. (Adapted from DARPA Neural Network Study Final Report, 1988.)

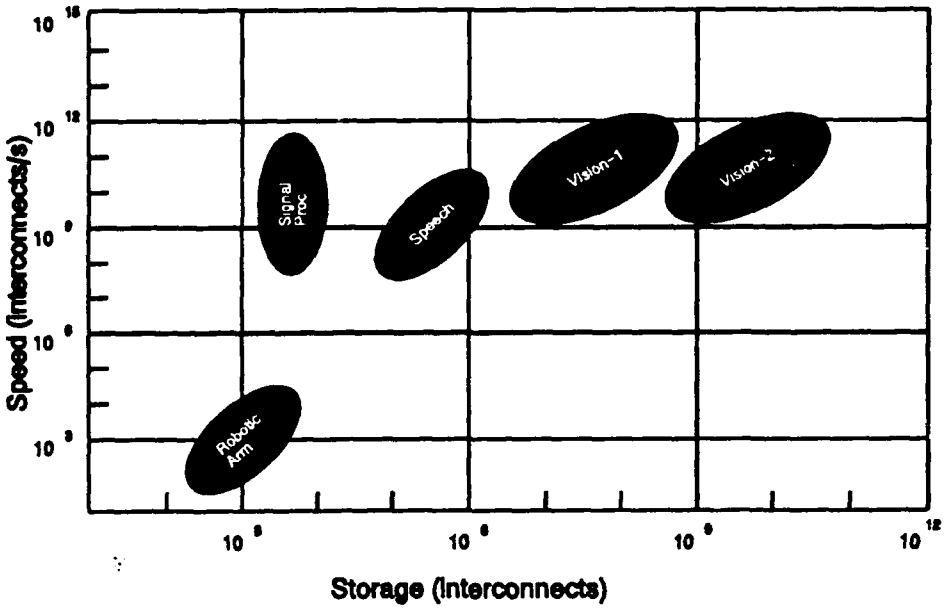

Figure 3. Estimated requirements for various neural network applications. (Adapted from DARPA Neural Network Study Final Report, 1988.)

2.2 Limitations of Existing Optical Interconnect Methods

Many methods have been proposed for using optics to connect large numbers of processors. In this section we will limit the discussion to methods which use free space propagation and transmission masks or holograms to connect 1D or 2D spatial light modulators (SLMs) with 1D or 2D detector arrays.

Three methods proposed for implementation of optical interconnects are shown in Figures 4, 5, and 6. Figure 4 shows a method studied by Farhat and Psaltis[5] for connecting two 1D arrays using a 2D transmission mask. Two cylindrical lenses (not shown) are used to diverge the light from the input array to all columns and to collect the light transmitted through each row of the mask. For input and output arrays of N elements each, N^2 transmission mask values are sufficient to specify all possible interconnections. For $N = 1000$, 10^6 interconnects can be implemented. Figure 5 shows how to obtain a large number of interconnects using a 2D hologram as the interconnect medium.[6] Although 2D SLMs and detector arrays can be used as the input and output respectively, unused areas must be maintained to avoid crosstalk in the output plane. This is due in part to the fact that the capacity of the interconnect medium scales as the area; this scaling relationship means the number of input and output elements scales as the linear size of the interconnect medium. This method thus has very similar capacity to that of Figure 4.

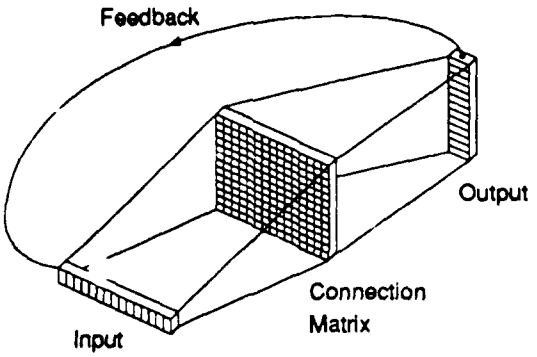

Figure 4. Connection of two 1D arrays using a 2D transmission mask.

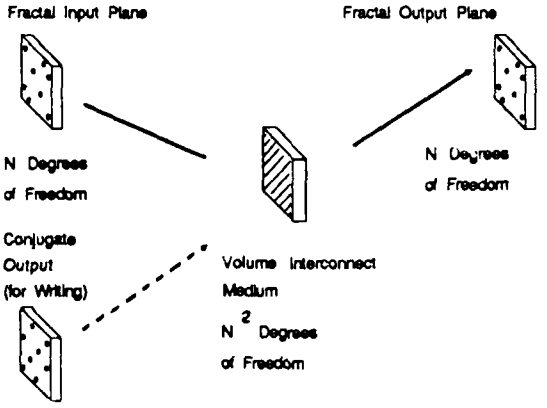

Figure 5. Connection of fractal patterns of dimension 1 on two 2D arrays using a 2D hologram.

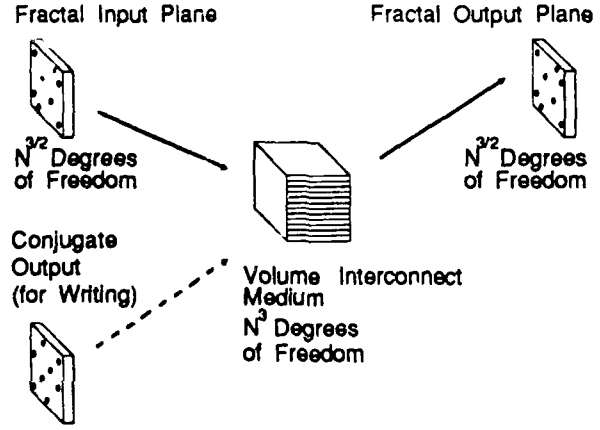

Figure 6. Connection of fractal patterns of dimension 3/2 on two 2D arrays using a 3D hologram.

2.2.1 Summary of the Fractal Input/Output Concept

A method capable of providing greater capacity is shown in Figure 9. In this case, a volume hologram is used to connect two partly-populated 2D planes. Since the number of interconnects scales as the hologram volume, the number of input and output states will scale as the 3/2 power of the interconnect hologram linear dimension.

Fractal patterns of dimension 3/2 have been proposed to supply the required dimensionality at the input and output planes.[7] The fact that some input and output positions must remain unused is easily seen from examination of Figure 9. Each connection between an input and an output state is recorded by a grating throughout the volume of the interconnect medium. The angular selectivity in the direction perpendicular to the Bragg planes is high, but it is low in the direction parallel to these planes. For this reason, inputs from the same row to certain outputs are not free from crosstalk and must not be used. This ambiguity is shown in Figure 7. Psaltis has shown in detail how this requirement leads to fractal patterns at the input and output.

2.2.2 Effective Utilization of SLM Capacity

The requirement to leave many states unused in the input and output planes leads to underutilization of the space-bandwidth product of the input SLM and of the detector elements in the output plane. The effect of this underutilization is illustrated in Table I for the case of volume hologram interconnects. The underutilization is not severe for small input/output arrays, but as the array size grows the penalty becomes worse and worse. For example, to achieve an equivalent system to the potential 4D concept to connect two 1000×1000 elements planes, SLMs with an area 100 times larger must be used.

This conclusion is unsatisfactory for two reasons. First, it hurts most for the implementation of large numbers of interconnects, exactly the area where optics should surpass electronics. Second, it wastes the precious commodity of space-bandwidth product (number of pixels) in the input SLM. Increasing this number has been a goal of a number of recent research programs, and thus the use of fractal input/output seems a step backwards.

The 4D interconnect concept proposed here overcomes this difficulty and should allow the implementation of much larger numbers of interconnects in a single device than 2D or 3D interconnect concepts. The use of fully-populated planes is well-matched to existing and projected input and output devices. In Section 5.2.6, we will present a compact optical design for a 10^{12} interconnect system.

2.3 The 4D Interconnect Concept

The 4D interconnect concept makes use of laser frequency to provide a fourth dimension in addition to the three spatial dimensions available in a volume hologram. This additional dimension allows the capacity of the interconnect medium to scale as the fourth power of the linear size of the interconnect medium. This scaling implies that the number of input and output states scales as the square of the linear size of the interconnect medium.

One way to achieve a 4D interconnect medium is to use a volume holographic medium in which volume gratings can be stored as a function of laser frequency. We believe a class of materials, known by various names, which we have chosen to call collectively spectral hole burning (SHB) materials, meets this need.[8] In these materials, the absorption can be reduced

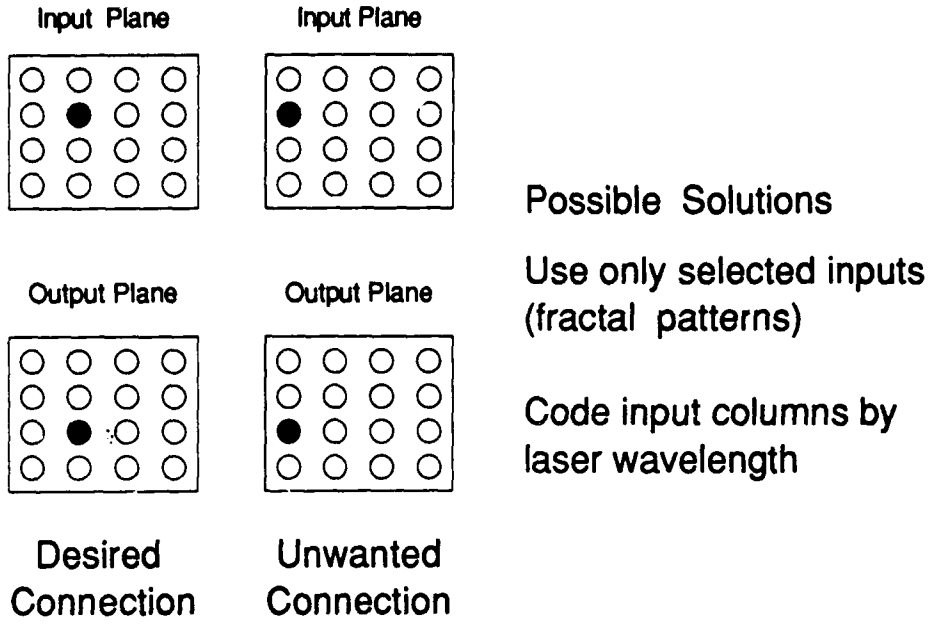

Figure 7. The crosstalk problem which occurs when using 3D interconnects. This figure shows two pairs of input/output points which are connected by the same volume grating.

Table I. Utilization of SLM Space-Bandwidth Product

Number of States N	Area A_1 (2D I/O) $\propto N$	Area A_2 ($\frac{3}{2}$D fractal I/O) $\propto N^{4/3}$	Area A_3 (1D fractal I/O) $\propto N^2$
4K	0.4 mm^2	6 mm^2	1600 mm^2
64K	7 mm^2	264 mm^2	4×10^5 mm^2
1M	1 cm^2	106 cm^2	10^6 cm^2
16M	16 cm^2	4295 cm^2	2.6×10^8 cm^2

Assumes 10 μm pixels

by illumination with light. At low temperatures, the homogeneous linewidth is much less than the inhomogeneous linewidth, and so a large number of independent holes can be burned, as shown in Figure 8. By using interference patterns to burn spatially varying patterns throughout the volume of an SHB material, holographic gratings can be recorded, *which are only seen by the recording wavelength.*

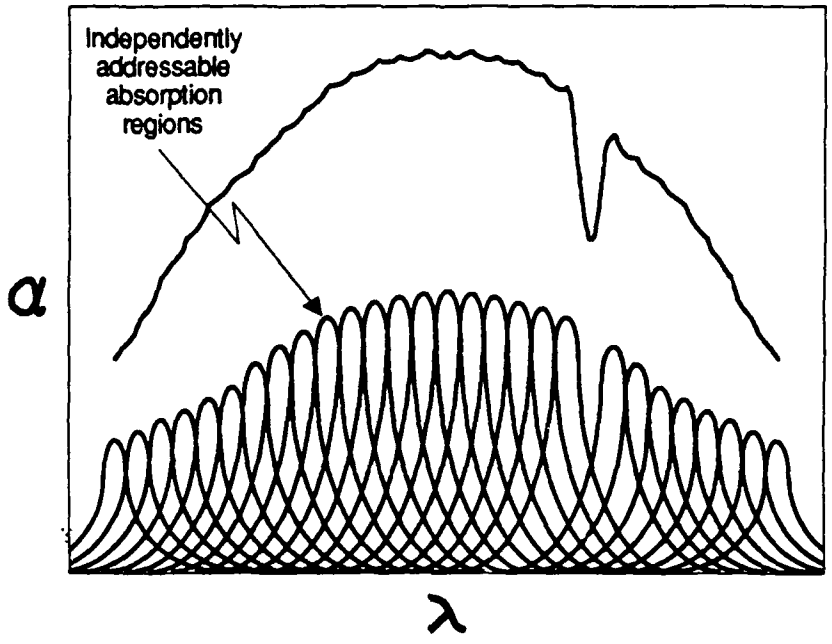

Figure 8. Spectral hole burning provides an additional dimension by allowing access to homogeneously broadened subpopulations of an inhomogeneously broadened absorber.

By properly organizing the inputs and outputs as a function of laser frequency and space, we can use fully-populated input and output planes. A schematic of this concept is shown in Figure 9. The network operates in two modes which we will call learning and calculating. In the learning mode, both the input and training planes are illuminated thus recording holograms in the interconnect medium. In the calculating mode, only the input plane is illuminated, and the radiation is diffracted to the output plane. In each case, the input plane is divided into columns, each illuminated by a unique laser frequency. Thus, although the Bragg selectivity is low when moving from column to column, crosstalk is prevented by this use of laser frequency.

At the output plane, the incident radiation at all wavelengths is summed incoherently. Any thresholding or other non-linearity required can be applied electronically. Because the outputs are non-negative either a bias level or dual-rail logic must be used.

We will discuss the architecture of a network in Section 5.2. Using simple feedback from the output plane back to the input plane, multi-layer networks can be realized. Introducing a second output plane corresponding to a reimaged input plane allows error signals to be propagated back through the network. This reverse use of the interconnect medium permits "backpropagation", a training method for multilayer networks,[9] to be implemented.

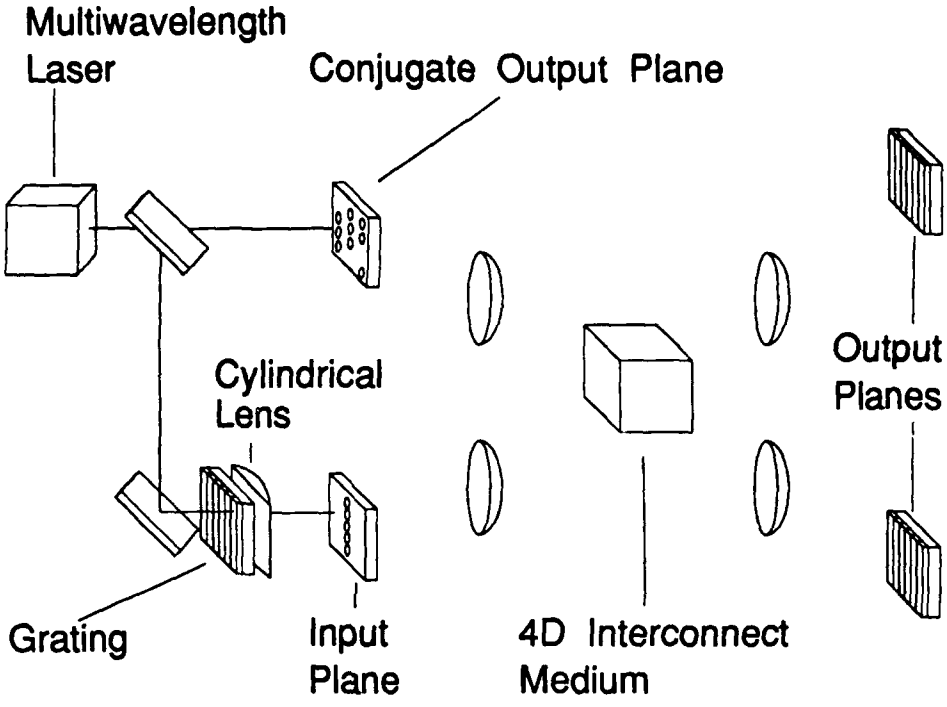

Figure 9. The 4D interconnect concept.

2.4 Key Issues for 4D Interconnects

In Phase I, we analyzed spectral hole burning materials for our application, examined the architecture and component requirements, and defined an experimental plan to be performed during Phase II.

The key issue to be addressed in Phase II will be an experimental confirmation of our Phase I analysis. We need to verify that the quality and diffraction efficiency predicted by our analysis can be achieved. A second issue is the confirmation of the material modeling effort required to predict the performance of SHB materials used to record refractive index holograms, as described in Section 5. Successful recording of refractive index holograms will be the key to greatly increased network capabilities. Finally, a demonstration of the performance of this type of neural network will be needed to begin the process of technology transfer planning, which will be essential for a successful Phase III.

3 Analytical Modeling of Spectral Hole Burning Materials

This section describes the results of Task 1 of our Phase 1 Statement of work, Spectral Hole Burning Material Analysis.

The fundamental and practical aspects behind the frequency channel structure and the recording of phase holograms are detailed. Computer models have been developed which permit an assessment of the capabilities of the approach. These models indicate that the resultant structures permit efficient phase hologram storage in SHB materials with a significant dynamic range.

3.1 Spectral Hole Burning

The concept of spectral hole burning (SHB) is best understood on the molecular level. A single molecule has a set of energy levels between which transitions are allowed. If the energy of the photon approximately matches one of the transition energies required, the photon can be absorbed by the molecule. If upon absorption, a chemical change to the molecule is induced, the absorption levels of the new molecule will not match the old ones. Therefore, the new molecule will not absorb light at the frequency of the first photon. In this way, the absorption capabilities of the molecule can be radically changed by exposure to light.

The width of the absorption peak is determined by the fundamental lifetime of the energy levels involved and the vibrations of the molecule and the medium in which it is contained. The resultant spectral width is called the **homogeneous** linewidth. At low temperatures, the broadening because of thermal effects can be reduced to 10 to 30 MHz.[10-14] Because of the highly periodic structure of a crystalline lattice, a large number of molecules will absorb at the same frequency when immersed in a single crystal. If the molecules are contained in a **glass** with little or no short range order, then each molecule sees a separate environment, providing separate absorption frequencies. This spread in frequency caused by the variation in molecular environment is known as the **inhomogeneous** linewidth and is generally quite large (10 THz or more[10]). (10 THz is about 12 nm wide at a wavelength of 600 nm.)

It is important to remember that the inhomogeneous absorption peak for a glass is composed of a large number of individual molecular populations which can be individually addressed by selecting the laser frequency (see Figure 10). Exposure at a single frequency which causes a photochemical change can effectively make the medium transparent ("burn a hole") in the medium over a narrow frequency range. The frequency width of the "hole" is simply the homogeneous linewidth of the medium.

This effect has been studied over the last 10 years in both organic and inorganic glasses and has been shown to be clearly observable with spectral widths ranging from 10 GHz at 77 K to 10 MHz at 1 K.[10] It has been previously shown by others that this approach could be used for storage of data via absorption holograms[15] and as bit-oriented spectral holes.[16] It has even been shown that multiple spectral holes can be made at the same frequency using different applied electric fields (i. e. Stark broadening).[17]

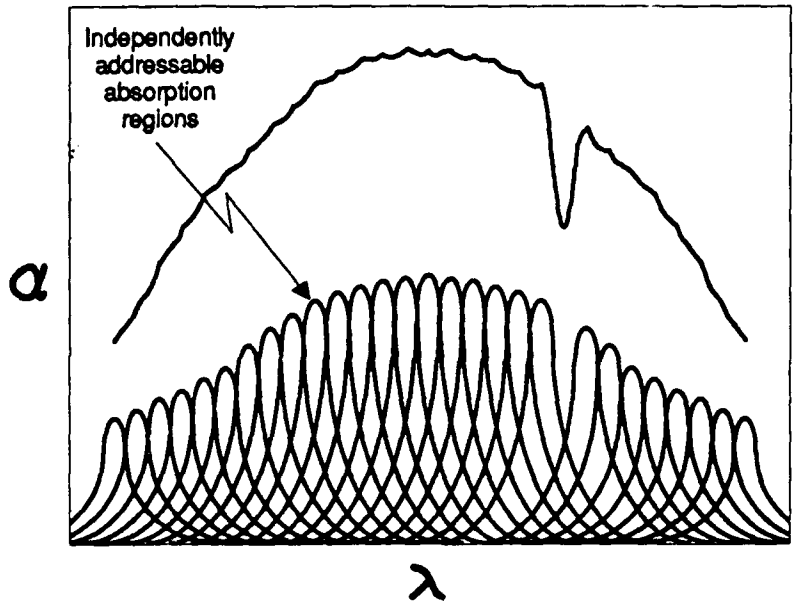

Figure 10. Schematic diagram representing the concept of individually selectable molecular populations within an inhomogeneously broadened spectral line.

3.2 Using the Real Part of the Refractive Index: Synopsis

The problem with spectral hole burning as it has been studied so far is that it is largely absorption-oriented. In a bit-oriented memory scheme this is ideal because it provides a "black and white" demarcation of the bit which relates directly to the measured light signal. Bit-oriented optical memories, however, are limited generally to an optical thickness of the material related to the depth of focus (and, therefore, resolution) of the optical system used.[18] Therefore, the full volume of a thick material (0.5 to 1 cm) is difficult to address. This same absorptive attribute also limits the efficiency of the holograms that can be stored (and therefore their number). This limitation can be seen from consideration of Kogelnik's coupled wave analysis[19] of mixed hologram efficiency. The expression he derived is shown below and indicates that the modulation of either the real or imaginary components of the refractive index can contribute to the efficiency (η) of the hologram.

$$\eta = [\sinh^2(\alpha_1 d/4\cos\theta) + \sin^2(\pi n_1 d/\lambda\cos\theta)]e^{-\alpha_o d/\cos\theta}, \qquad (1)$$

where

α_1 = the modulation in the absorptivity,

α_o = the average absorptivity of the material,

n_1 = the modulation of the real component of the refractive index,

θ = the half angle between the incident and reference beam used to create the hologram, and

d = the thickness of the holographic medium.

If the holographic material has any average absorptive properties, then the overall efficiency of the hologram will be directly limited by simple absorption effects through the exponential term in equation (1). Consideration of these inherent absorptive effects cause absorption holograms to be limited to 3.7 percent efficiencies, while phase holograms (stored in non absorbing materials) can reach efficiencies of 100 percent. In fact, if the dynamic range of the index modulation is large enough, multiple holograms, each of 100 percent efficiency, can be stored in the same material at the same wavelength.

When one considers the storage of multiple holograms of modest efficiency (less than 1 percent) the quadratic terms in equation (1) simplify to being proportional to simple squares of the real and imaginary index modulations. Given this relationship we find that the hologram efficiency declines as $1/N_H^2$, where N_H is the number of holograms stored. This can be seen to limit the number of holograms which can be stored directly. If a hologram efficiency of 10^{-5} is required, equation (1) will permit the storage of only 60 absorption holograms. If the dynamic range of the real component of the refractive index permits the storage of a single 100 percent efficient hologram, then 316 holograms can be stored. Because the phase hologram approach has no fundamental limit (other than practical material property considerations), the number of phase holograms which can be stored is virtually unlimited. The key is to then explore material approaches which permit phase hologram storage and have the potential for large dynamic ranges.

Both bit-oriented and holographic memories based on absorption require large amounts of light to be absorbed during reading operations rapidly causing erasure of the data. Refractive index modulation (phase) holograms do not suffer from these problems. They have the ability to diffract the light without significant absorption. Using holograms permits data storage in depth, and using the real part of the refractive index permits reading of data without erasure; these are two critical factors in achieving a truly enormous data density in a useful system.

The Kramers-Kronig relation[20] expresses the direct relationship between the real (refractive) and imaginary (absorptive) parts of the dielectric constants of a material (and therefore the real and imaginary parts of the refractive indices). For a single absorption line the relation is seen in Figure 11. Because of a spectral absorption at a single homogeneously broadened frequency the refraction is altered in the near vicinity of the absorption peak. The key point to be noted is that the absorption falls off more rapidly than the refractive effect. If the absorption could be modulated spatially, one could read a phase hologram when the reading frequency is off resonance and an absorption hologram when on resonance. If the modulation is large enough and the absorption at the reading frequency low enough, near 100 percent efficiency is possible with phase hologram storage.

If the absorption peak is made wider by using a multiplicity of populations centered over a range of frequencies, then the real part of the refractive index can be enhanced near the absorption edge. The effect is logarithmic with frequency width, but the effect can be large enough to make the peak of the real part of the refractive index modulation even larger than the peak of the imaginary part (see Figure 12). The locations of the peaks of index and absorption modulation, in frequency space, are still shifted relative to each other, allowing reading in a low absorption region of the spectrum. This structure can be replicated many times in frequency space and each structure can be accessed independently simply by changing the illumination frequency.

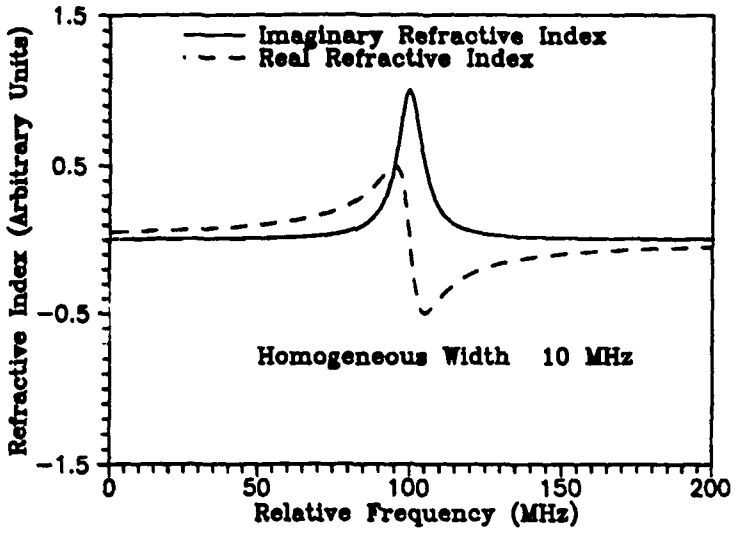

Figure 11. Real and imaginary components of the refractive index for a single damped oscillator. Note that the real part has a range that extends well beyond that of the imaginary component.

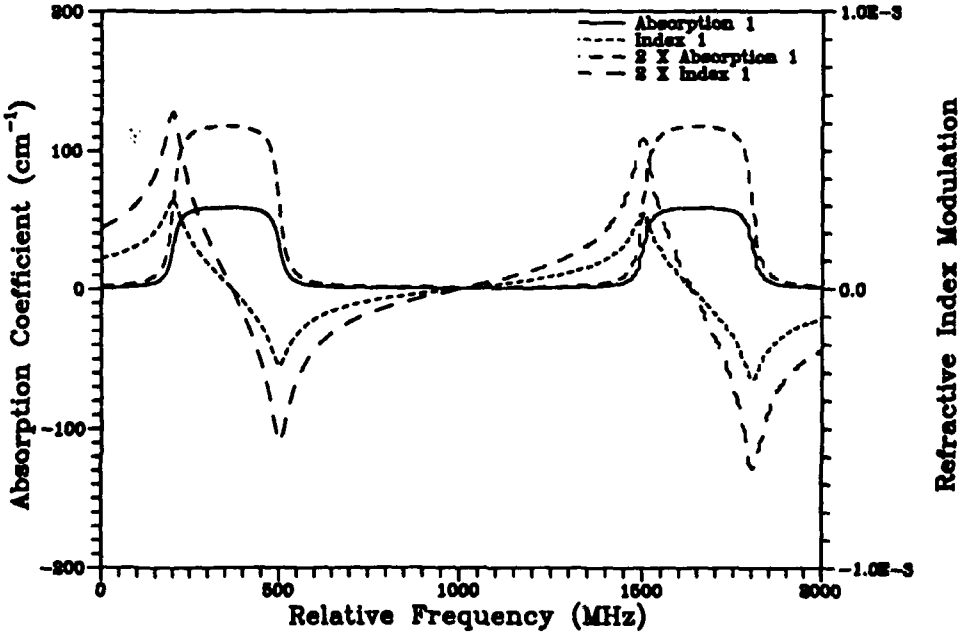

Figure 12. Schematic of two adjacent absorption structures showing the modulation of the resultant refractive index. Such a structure is possible with porphyrin in polyethylene at 4 K. The frequency coordinates of this structure will essentially scale as $T^{1.3}$.

Writing and reading can (and should) also be done in the low absorption tail. Absorption in the tail will induce photochemical changes to molecules located throughout the broad population peak. Because the absorption is low, however, it permits modulation of the molecular populations

(and therefore the refractive index) through the depth of the material, permitting highly efficient and selective holograms to be generated. It therefore permits one to "tap the resources" of a large molecular population without being completely absorbed by it.

Increased access is allowed by adding more degrees of freedom (dimensionality). Storage as a function of frequency can provide such access. The frequency channel structures shown in Figure 12 are best viewed as access paths into and out of the material for reading and writing purposes. Without these channels, the material would be too opaque to permit reading or writing. Without the adjacent absorption structures, the material would have inadequate storage capacity to realize the ultimate capacity of volume media. By structuring the material in frequency space, the material has been separated into sections permitting access and sections permitting storage.

3.3 Detailed Modeling of Frequency Channels

To gain an appreciation as to whether the frequency channel approach is of practical value, it is important to perform some detailed modeling of the key aspects of the approach. The two key issues which have been examined in detail are

1. What is the magnitude of the refractive index modulation possible in a frequency channel structure of suitable dimensions?
2. Can such a structure be created in a manner which is practical and yet provide the performance desired?

These two issues are addressed by the analyses and computer modeling shown below.

3.3.1 Index Modulation Near an Absorption Band Edge

If a single molecule is modeled as a harmonic oscillator with a small amount of damping, one can derive functions describing the real $(1 + n_1)$ and imaginary (k) parts of the refractive index. (The imaginary part of the refractive index is related to the absorption coefficient (α) by the formula $\alpha = 4\pi k/\lambda$, where λ is the wavelength of light used.)

$$k(f, f_r) = \frac{K}{2f_r} \frac{\Delta f}{(\Delta f/2)^2 + (f - f_r)^2} \tag{2}$$

$$n_1(f, f_r) = \frac{K}{f_r} \frac{f - f_r}{(\Delta f/2)^2 + (f - f_r)^2} \tag{3}$$

where Δf is the homogeneous spectral width of the absorption, f_r is the resonance frequency of the oscillator, and f is the frequency of illumination[20]. The constant K is determined by the fundamental properties of the molecule. These functions are plotted in Figure 11 and show that the absorption falls off much more rapidly than the real part of the refractive index.

The formulae to be derived here represent a population of oscillators whose central frequencies are distributed over a finite range between f_1 and f_2. A simple case will be used where the population density is a step function within the range and zero everywhere else. Upon integration we find that the formulae for the imaginary and real parts of the refractive index are simply

$$k(f) = K[\tan^{-1} \frac{2(f - f_2)}{\Delta f} - \tan^{-1} \frac{2(f - f_1)}{\Delta f}] \tag{4}$$

and

$$n_1(f) = -\frac{K}{2} \ln \frac{(f - f_2)^2 + (\Delta f/2)^2}{(f - f_1)^2 + (\Delta f/2)^2}. \tag{5}$$

It is equations (4) and (5) which are plotted in Figure 12 (k has been transformed into its equivalent absorption coefficient value in that figure). This derivation represents a first order representation of a potential memory structure in frequency space.

The magnitude of the index modulation can then be directly translated into the phase hologram efficiency as is done in Figure 13. From the index modulations seen in Figure 12 we can see that the efficiency of the phase hologram(s) which are stored can be quite substantial. An index modulation of 10^{-4} in the real component of the refractive index would seem readily obtainable in a frequency range where the absorption is acceptably low (less than 10% or lower absorption). When inserted in a material which is 1 cm thick, the dynamic range permits storage of 3 holograms of 90% efficiencies (efficiencies which are limited only by the modest absorption within the frequency channel). This clearly will permit a significant storage capacity.

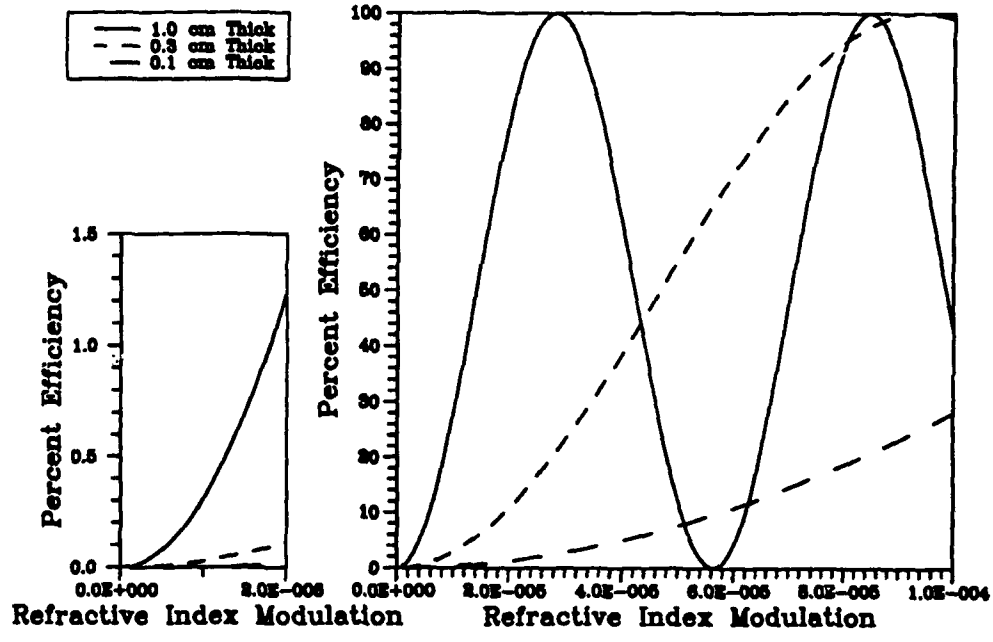

Figure 13. This diagram relates the magnitude of the modulation of the real component of the refractive index to the efficiency of the phase holograms which can be stored in the material. Several thicknesses of material are shown for comparison.

3.3.2 Creation of Frequency Channels in SHB Materials

In the above analysis, the means by which the frequency channel was created was largely ignored. It was simply assumed that the frequency channels could be completely bleached and had molecular distributions which could be represented by step functions. These theoretical simplifications are useful as a first approximations and could represent adequate representations of the actual performance under certain circumstances. Such a circumstance would be one where the channels are created at a temperature lower than the operating temperature, with a very narrow linewidth laser, and with a large amount of time used in their creation. However, these circumstances may be impractical (or at least cumbersome). To model the effects of a more realistic channel creation process we have developed a model which takes into account the finite properties of the laser and homogeneous linewidths of the SHB material, as well as the limitations on the ability to bleach the material.

The bleaching process is characterized by the relationship

$$\frac{dN}{dt} = \frac{-N}{h} \in < t_{-\infty}^{\infty} \sigma(f, f_r)\, P(f, f_b)\, df \tag{6}$$

where

N is the instantaneous number density distribution of molecules,

t is time,

h is Planck's Constant,

f_r is the molecular frequency,

f is the frequency of a photon,

$\sigma(f, f_r)$ is the molecular absorption cross section distribution function,

f_b is the instantaneous centerline frequency of the laser, and

$P(f, f_b)$ is the instantaneous power density distribution function of the laser.

The molecular absorption cross section is again assumed to be a Lorentzian function,

$$\sigma(f, f_r) = \frac{\sigma_o}{\pi} \frac{\Delta f_r/2}{(\Delta f_r/2)^2 + (f - f_r)^2} \tag{7}$$

where

σ_o is the total absorption cross section of the molecule and

Δf_r is the homogeneous linewidth of the molecule.

We shall assume that the process of creation of the frequency channels is one of simply sweeping the laser (as a function of frequency) across the frequency channel. The power density distribution of the laser will also be described by a Lorentzian function:

$$P(f, f_b) = \frac{P_o}{\pi} \frac{\Delta f_b/2}{(\Delta f_b/2)^2 + (f - f_b)^2} \tag{8}$$

where

P_o is the instantaneous irradiance of the laser beam and

Δf_b is the linewidth of the laser beam.

The population density after hole burning may be obtained by combining equations (6), (7), and (8); as *

$$\frac{N}{N_o} = \exp\left(\frac{-\sigma_o P_o}{h} \cdot \frac{1}{\pi} \int_{t_o}^{t_f} \frac{\Delta f_b/2 + \Delta f_r/2}{(\Delta f_b/2 + \Delta f_r/2)^2 + (f_b - f_r)^2}\, dt\right) \tag{9}$$

after evaluating the frequency integral in equation (6).

Phase hologram storage would be expected to be most effective when the edges of the channels are sharp relative to their width. In order to achieve the desired sharpness, both the linewidth of the burning laser and the homogeneous linewidth of the material must be small compared to the width of the channel. Assuming a constant slew rate during the creation of the channel leads to,

$$f_b = f_o + f_b'(t - t_o) \tag{10}$$

where

f_o is the initial frequency of the laser beam and

f_b' is the frequency slew rate.

Combining equations (9) and (10) and evaluating the integral,

$$\frac{N}{N_o} = \exp\left(\frac{-\sigma_o P_o}{h f_b'} \cdot \frac{1}{\pi}\left(\arctan\left(\frac{f_f - f_r}{\Delta f_b/2 + \Delta f_r/2}\right) + \arctan\left(\frac{f_r - f_o}{\Delta f_b/2 + \Delta f_r/2}\right)\right)\right) \tag{11}$$

where f_f is the final frequency of the laser beam.

In the above N/N_o is simply the depletion ratio (the fraction of molecules which remain after the channel burning process) at a particular frequency (see the lower section of Figure 14). The first factor in the exponential function, $-\sigma_o P_o / h f_b'$, effectively defines the asymptotic limit of the depletion ratio for infinitely wide channels. This term predicts, as expected, that a deeper channel can be created by increasing the power of the burning laser or by slewing more slowly.

Full exploitation of the frequency channel approach requires that multiple frequency channels be burned into the material. The effect of burning several channels may be computed from the relationship:

---

* This formulation assumes that the laser operates at constant power from time t_o to time t_f. For cases in which this assumption is invalid, equation (9) is replaced by the equation

$$\frac{N}{N_o} = \exp\left(\frac{-\sigma_o}{h} \cdot \frac{1}{\pi} \int_{t_o}^{t_f} P_o \frac{\Delta f_b/2 + \Delta f_r/2}{(\Delta f_b/2 + \Delta f_r/2)^2 + (f_b - f_r)^2}\, dt\right)$$

and the subsequent analysis is somewhat more complicated. However, this equation can be directly integrated numerically.

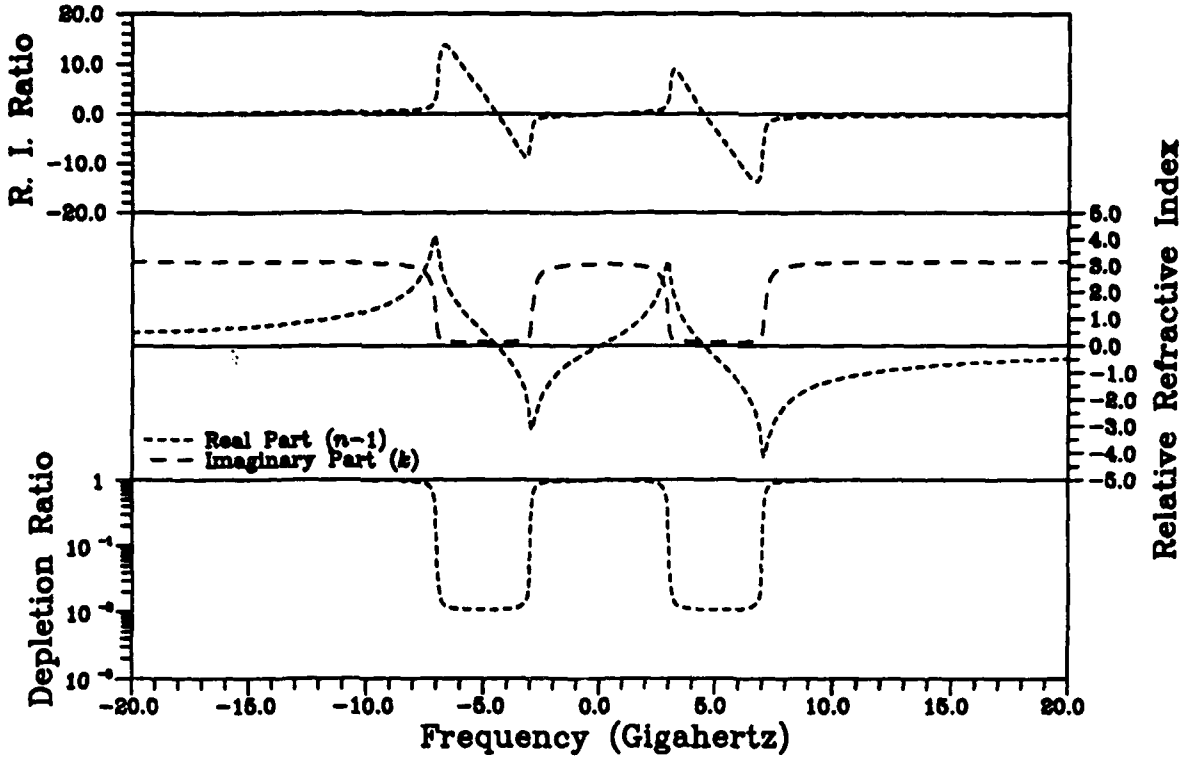

Figure 14. Calculated optical properties of a realistic model for a frequency channel structure. The laser linewidth and homogeneous linewidth are both 100 MHz.

$$\frac{N_m}{N_o} = \prod_{i=1}^{m} \frac{N_i}{N_{i-1}} \tag{12}$$

where

m is the number of channels,

i is the channel index, and

N_i is the molecular number density distribution after i channels have been burned.

If we assume that each channel is burned independently (i.e. there are no complicating physical phenomena which limit us) we can readily combine equations (11) and (12) as

$$\frac{n}{n_o} = \exp\left(\frac{-\sigma_o P_o}{h f_b'} \cdot \frac{1}{\pi} \sum_{i=1}^{m} \left(\arctan\left(\frac{f_f^{(i)} - f_r}{\Delta f_b/2 + \Delta f_r/2}\right) + \arctan\left(\frac{f_r - f_o^{(i)}}{\Delta f_b/2 + \Delta f_r/2}\right)\right)\right) \tag{13}$$

where

$f_o^{(i)}$ is the initial frequency of the laser beam for the $(i)^{\text{th}}$ channel and

$f_f^{(i)}$ is the final frequency of the laser beam for the $(i)^{\text{th}}$ channel.

The characteristics of equation (13) are similar to equation (6), with the summation of arctangents always falling between 0 and π as long as the frequency channels are distinct.

3.3.3 Refractive Index Characteristics After Channel Formation

The magnitudes of the real and imaginary components of the refractive index can be directly calculated (using equations (1) and (2)) once the molecular distributions are provided by equation (13). Unfortunately the resulting expressions are not readily integrated through analytic techniques and therefore must be evaluated numerically. These results can be seen represented in the middle segment of Figure 14 and show that the major qualitative and quantitative aspects of the refractive indices are retained when compared with Figure 12.

From an examination of equation (1) we can see that the key factor to be considered here is not the absolute value of the index modulation which is possible (we have already shown that the magnitude is quite substantial for thick materials) but the relative magnitudes of the real and imaginary components. By keeping the ratio (R.I. Ratio) of these components high it is possible to have significant phase modulation with acceptable absorption losses. From an examination of the upper segment of Figure 14 it can be seen that the ratio can easily attain magnitudes of over well over 10. This magnitude for the ratio is rather important. By reference to equation (1) and knowing that $\alpha = 4\pi k/\lambda$ we can immediately realize some reasonable performance capabilities. If α is defined so as to permit 50 percent transmission in a 1 cm thickness, then we find that the real component of the refractive index can take on a magnitude of about 3.3×10^{-5}. From Figure 13 this translates into a phase hologram efficiency of 100 percent which is then attenuated to 50 percent by simple absorption. In this way, the storage capacity of the material has been increased at a single frequency when compared with simple absorption holograms. Similarly, if the refractive index ratio is increased further, one can reduce absorptive losses almost proportionately, thereby increasing storage capacity, or reducing heat absorption by the SHB material. These tradeoffs can now be made to suit the specific operational needs of the 4D neural net system.

3.3.4 Computer Simulation and Results

SPARTA has implemented a computer simulation of the spectral hole burning process. This simulation was designed so that additional effects, such as non-uniform initial molecular distributions and non-constant values of the constant K in the above analysis can readily be integrated and evaluated in conjunction with a follow-on effort. Figures 15, 16, and 17 show representative output from this simulation for the creation of multiple channels in a material having a homogeneous linewidth of 100 MHz using a laser with a linewidth of 100 MHz.

The refractive index ratio (R. I. Ratio) describes the ratio of the modulated real part of the complex refractive index to the imaginary part of the complex refractive index. The most striking result of these modeling efforts is that the refractive index ratio peaks at a well-defined frequency when a realistic absorptivity remains unbleached in the channel. This points to a clearly defined frequency at which optimal hologram readout should take place. (Such a clear choice of optimal frequency was not available from the simple analysis of a completely bleached channel.) The consideration of the optimal writing frequency is not so clear because the specific system needs may affect the choice. If the absorptivity within the channel is selected to be low, so as to minimize heating of the material during writing, it would be advantageous to adjust the

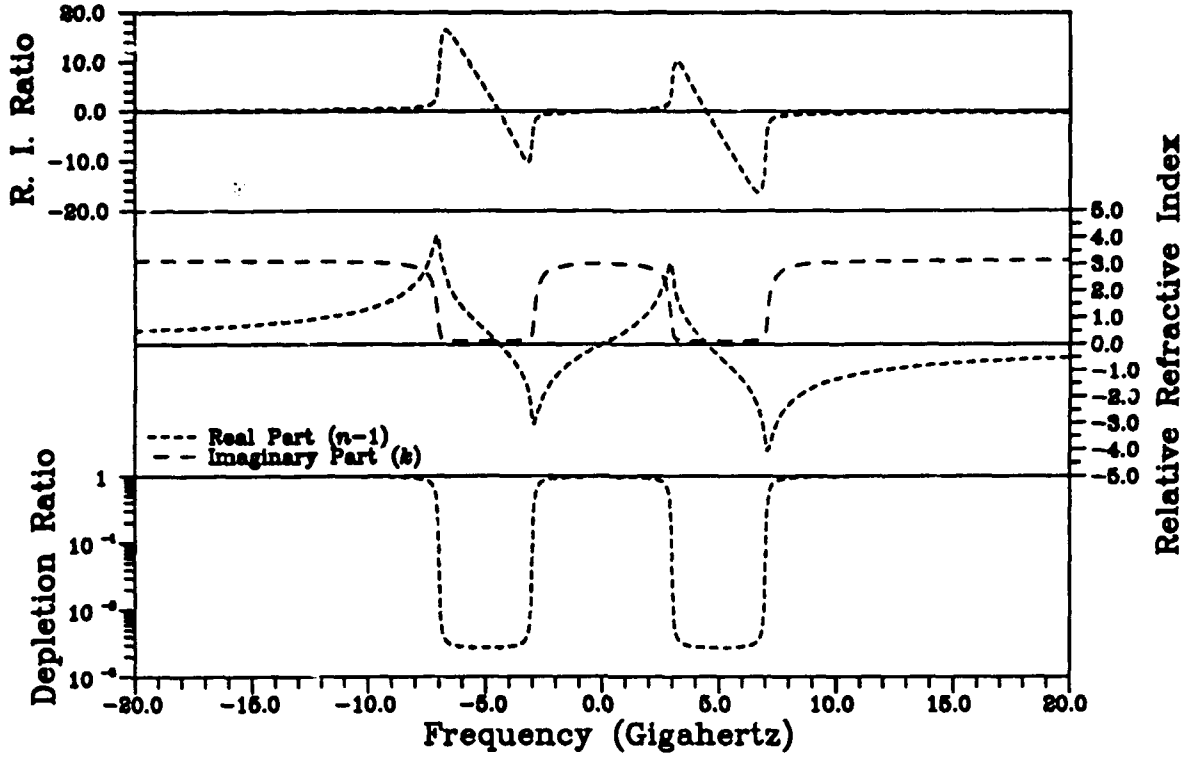

Figure 15. Calculated performance of the frequency channel structure assuming that the channel is bleached to a greater depth.

laser frequency to a slightly more absorbing frequency (toward the absorption edge). This would permit a more efficient use of the writing power of the laser. These kinds of considerations show the extra freedom in system design which can be gained through use of the frequency channel structure.

These figures also show that increasing the depth of the frequency channel (reducing the depletion ration by increased bleaching) seems to have modest influence over the R.I. Ratio. Adding extra channels does not change the fundamental features of the structure, and increasing the spacing between channels does not markedly increase the R.I. Ratio above 15. We do note that increasing the spacing between channels (see Figures 16 and 17) does have a noticeable effect upon the influence which adjacent structures have on each other. This influence between adjacent structures is effectively a measure of the level of crosstalk between frequency channels. In a later section of this document we shall determine that an acceptable level of crosstalk is of the order of 1 part in 20. Since the magnitude of the crosstalk is proportional to the square root of the index modulation effects, we only require that the influence between structures be reduced to 1 part in 4.5. This translates into a spacing between these structures of the order of 3 GHz. If we arbitrarily increase the spacing to 10 GHz in order to keep the R.I. Ratio of the order of 20, we will clearly have low crosstalk and high hologram storage capacity.

The subject of storage capacity will be discussed more fully in the section on photon budgets. However, if we set the absorptivity so as to permit approximately 60 percent transmission, we can see that an R.I. Ratio of 20 permits as many as 641 holograms to be stored at a single

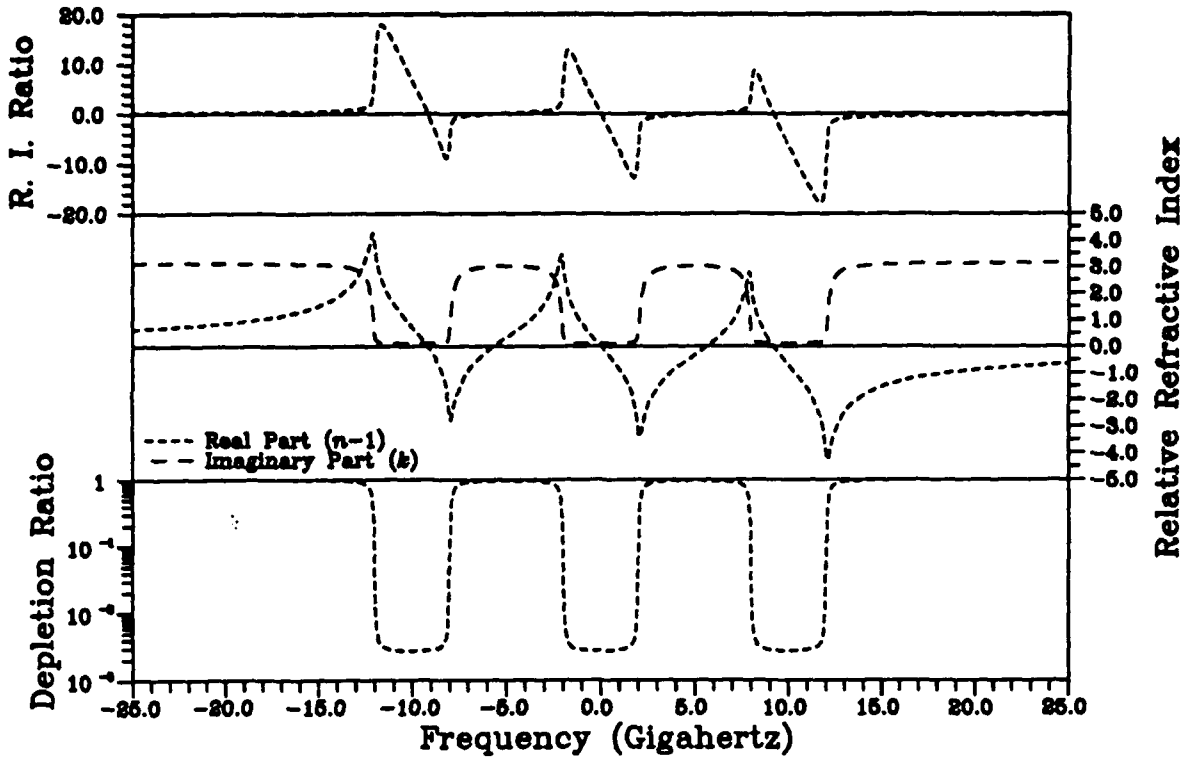

Figure 16. Calculated performance of the frequency channel structure showing how the increase in number of channels effects the index modulation.

frequency. If the spacing between channels is 10 GHz, 10^6 holograms can be readily stored within a frequency range of 20 THz (20 nm). This storage capacity is considered to be quite acceptable, and it also leads to the possibility of high efficiency hologram storage for certain applications. Naturally, if the homogeneous line width were reduced below 100 MHz (and the laser linewidth were similarly reduced) the spacings between channels and the total frequency range required would be reduced. For example, if the homogeneous linewidth were 40 MHz (H_2P in polyethylene) and the laser linewidth were reduced to 10 MHz or less, the spacing between channels could be as little as 3 GHz and the frequency range of the material would need to be only 6 THz (6 nm) (which is less than the inhomogeneous linewidth for this SHB material).

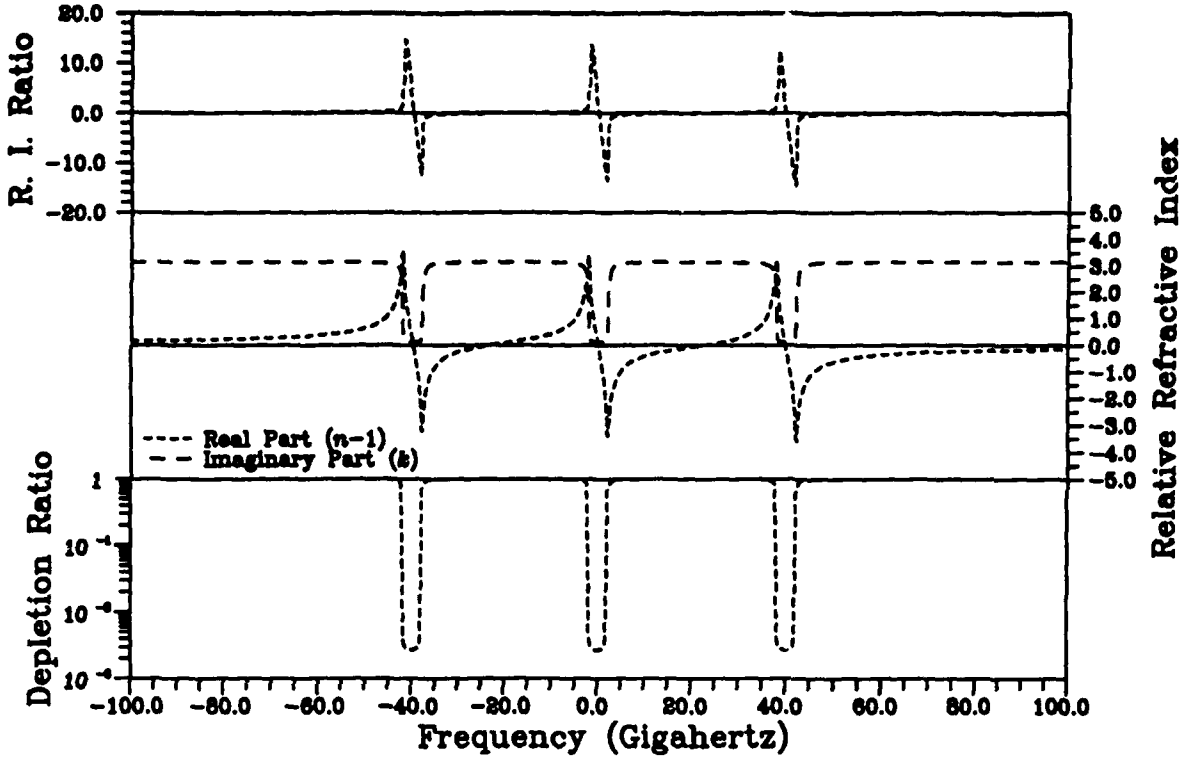

Figure 17. Calculated performance of the frequency channel structure showing how the increase in spacing between channels reduces modulation crosstalk effects. Crosstalk is noted to be reduced because the index modulation at each channel is nearly unaffected by the presence of adjacent channels.

4 Architecture Requirements

This section describes the results of Task 2 of our Phase 1 Statement of Work, Determine the Architecture Requirements.

4.1 Equivalence of Neural Networks

Many different types of neural networks have been proposed and simulated or implemented. The different network structures are associated with different applications. Hopfield networks are symmetric structures ($T_{ij} = T_{ji}$) in which the output is fed back to the input. They have been used to solve optimization problems such as the traveling salesman problem.[21] Single layer networks perform a voting operation and have been used to learn simple discrimination tasks.[22] Networks with hidden states can be used to solve certain logic problems, such as as XOR, that cannot be solved using single layer networks.[23] Multilayer feedforward networks have been used to solve classification problems such as text to speech.[24] A number of simple network types are illustrated in Figure 18.

Our goal was to determine how our 4D interconnect method could be used to implement as many different types of network as possible. This flexibility would allow us to apply our technique to more problems. In the process of examining this issue we discovered a general architecture which can implement all of these network types and probably many more.

The first step in this process was to realize that many networks which appeared to be different could really be considered to be equivalent. For example, a network structure with a hidden state, of the same form as that used to solve the XOR problem, is shown in Figure 19. By adding several "pass-through" and "unused" states this network can be made to look like a "regular" multilayer network. The term regular refers to the fact that each layer has the same number and density of states. The "pass-through" states have a linear rather than sigmoidal input-output relationship. A single layer network with arbitrary feedback can be recast as a two-layer network with parallel feedback as shown in Figure 20. Finally, a multilayer network can be implemented in a single-layer structure if parallel feedback from the output to the input is allowed, as shown in Figure 21.

By recasting networks using "dummy" states, "pass-through" states, additional layers to simplify feedback, and parallel feedback from output to input, networks of arbitrary complexity can be reduced to a single layer network with parallel feedback from sections of the output plane to other sections of the input plane. It is relevant to note that, in theory, a three-layer network is sufficient to achieve any arbitrary decision region in N-dimensional hyperspace.[25] Thus real networks will be limited in complexity.

4.2 Requirements for Backpropagation

Backpropagation is a training method for multilayer feedforward networks.[26] It solves the problem of how to adjust the weights associated with the hidden layers of a network given knowledge of only the inputs, outputs, and desired outputs of the network.

Conceptually, the backpropagation algorithm is quite simple. Within any layer the weights are modified proportional to the outer product of the input to the layer and the errors at the output. The errors are obtained by subtracting the desired output from the actual output. The residual errors are then propagated back to the previous layer by using the interconnections in

a. Single Layer, Feed Forward

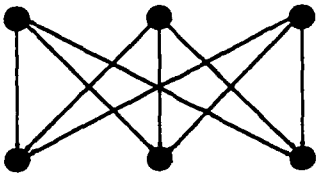

b. Single Layer, Direct Feedback

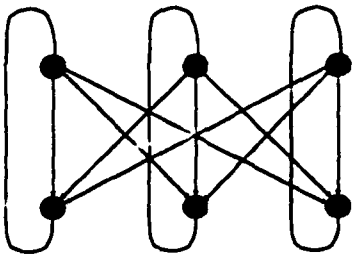

c. Multilayer, Regular, Feed Forward

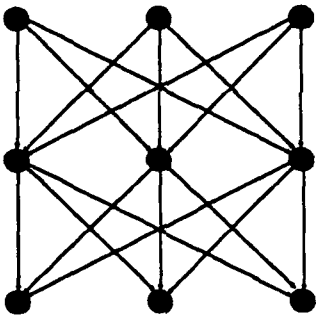

d. Not Layered

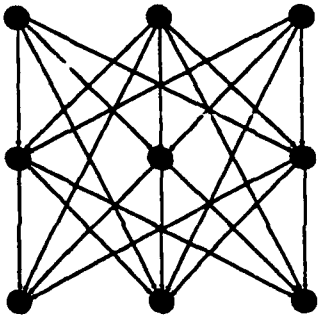

Figure 18. Simple network types.

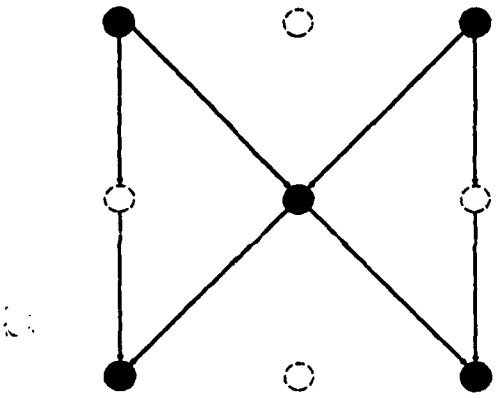

Figure 19. Network with a hidden layer to perform the XOR logic operation.

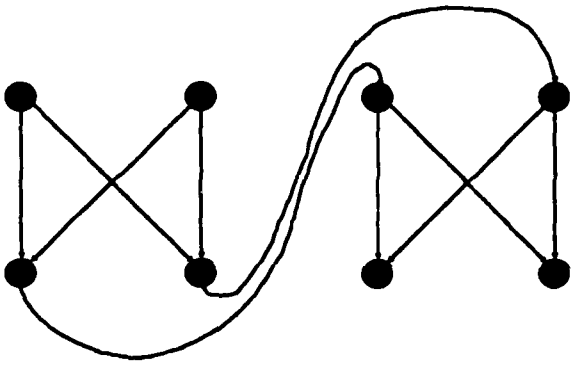

Figure 20. A single layer network with arbitrary feedback recast as a two-layer network.

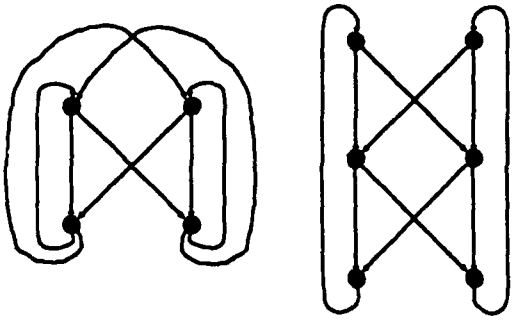

Figure 21. A multilayer network can be recast as a single layer network with parallel feedback from some sections of the output to other sections of the input.

reverse. The effect of the non-linear states is reversed by applying the derivative of the non-linear (normally sigmoidal) function. The process is then repeated for this previous layer.

Holographic interconnects are well-suited to implementation of backpropagation. The mathematics of backpropagation using holographic interconnects have been presented by Wagner and Psaltis.[27] If the inputs and errors are presented simultaneously to a network at the input and training planes, gratings proportional to the outer product are recorded. It has also been shown that grating strengths can be decreased by recording gratings 180° out of phase with the original recording.[28]

A configuration for using the 4D interconnect medium for backpropagation is shown in Figure 22. In this architecture the arrows pointing from left to right are optical signals, while the shaded arrows pointing from right to left are electronic signals. The output plane is in the image plane of the training plane, and the backpropagation plane is in the image plane of the input plane. Initially, optical signals from both the training plane and the input plane are used to write interconnects by recording holograms in the 4D interconnect medium (in the center of the figure). The interconnects can then be used by turning off the training plane and measuring the signals at the output plane in response to signals applied to the input plane. Electronic feedback from the output to the input, as shown by the top path, can be used to create multilayer network structures. Training the network requires error signals which can be propagated backward through the network. These error signals are obtained by subtracting the actual output from the desired output at the output plane. The diagonal path provides the feedback required for the first stage of backpropagation. In backpropagation the network is "used in reverse," and this effect can be achieved by presenting the errors to the network at the training plane (bottom left) and measuring the outputs at the backpropagation plane. Working backward through the network is achieved by the lower electronic feedback path, which mirrors the top path used to achieve a multilayer network in the forward mode.

One important difference is the method of preventing crosstalk. When using the network in a forward configuration this is accomplished by coding the input columns by wavelength and incoherently summing all the wavelengths at each output position. When using the network in reverse, each error input potentially contains all wavelengths, and the backpropagated errors must be selected by wavelength in each column. Because a color filter performing this separation may be difficult to fabricate (because of the small wavelength separation) it may be necessary to present each wavelength to the network separately. This may slow the learning process but presents no conceptual difficulty. We believe the derivative of the non-linearity can be applied electronically, as discussed in the next section, however, Wagner and Psaltis have discussed how this might be achieved optically.[27]

4.3 Utility of Electronic Feedback

We plan to implement the feedback function, required for implementation of arbitrary multilayer networks and learning, electronically.

For reasons which will become clear in this section, we choose to include the sigmoidal nonlinearity and its derivative in the electronic part of the network. The flexibility of electronics provides advantages for an initial implementation, but there are also reasons to believe this choice makes sense in the long run. We will present these reasons in this section.

First, the simple nature of the feedback function we have defined is well-suited to electronic

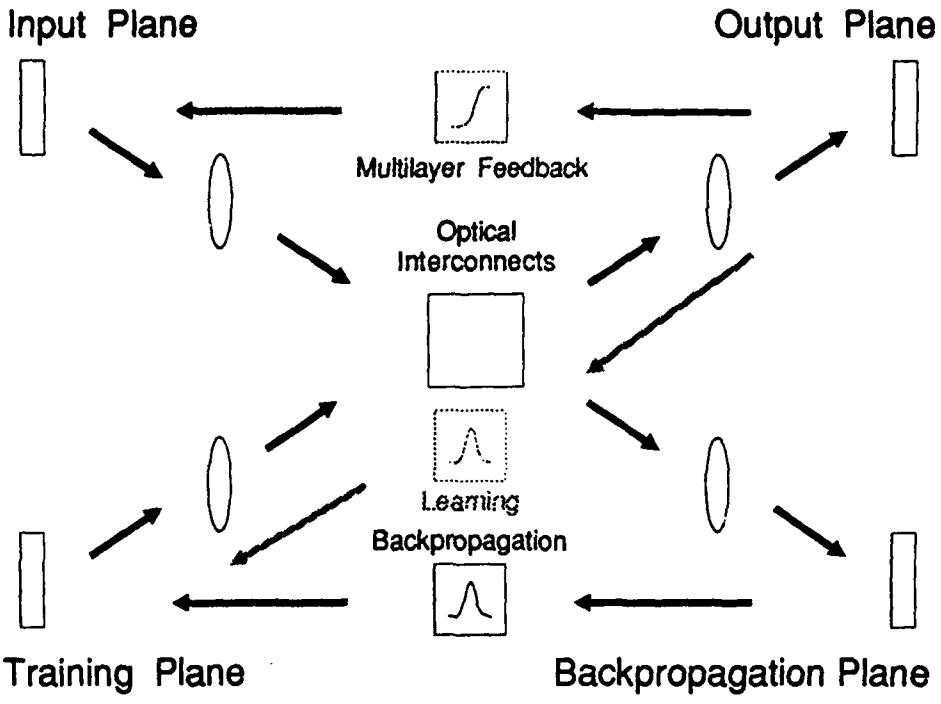

Figure 22. Strawman architecture for an artificial neural network computer, showing a configuration for backpropagation using the 4D interconnect medium.

data transfer. Direct, parallel feedback requires a one-to-one connection of contiguous elements from one part of the output plane to a set of contiguous elements in the input plane. Detector arrays have been developed for machine vision applications which can be read out in subsections.[29] Direct memory access techniques can be used to write directly to the memory buffer of a display device. This data transfer can be performed at rates equal to those accepted by current and projected spatial light modulators and should not limit the performance of the network.

Second, the computation requirements of the feedback loop are much less than those of the interconnect section of the network. For $N \times N$ input and output planes, the interconnect operations can require as many as $2N^4$ multiplies and adds. The neuron and feedback operations will only need to be performed once for each pixel and thus will require N^2 operations. The ratio of these requirements, $2N^2$, can be as large as 2×10^6 for $N = 1000$, and thus the payoff for optical implementation of the feedback function is tiny compared to the payoff for optical interconnects. Since the feedback computations require only three functions; a sigmoid, a sigmoid derivative, and a pass-through function, these computations can even be implemented using dedicated digital or analog circuits to achieve data rates as high as 50 MHz. The flexibility of electronics to implement any of these three functions simplifies and unifies the thinking and learning modes of the network.

Electronic implementation of the non-linearity also makes sense from an energy standpoint. It is well known that optical implementations of switching require more energy per operation than their electronic equivalent.[30] This fundamental limitation of optics can be understood in simple terms by observing that electrons interact with one another, but photons do not. Thus

any non-linear "photonic" operations require that electrons be involved, for example, through electro/optic effects or medium polarization (χ^2 and χ^3 effects in materials). For purely optical implementation at least some photons must undergo a photo-electron conversion after which the electrons undergo a non-linear interaction. The additional conversion step, not required in electronic computing, results in increased energy requirements.

Finally, in practical implementations of multilayer networks, gain will be required to compensate for optical losses. Optical gain is also difficult to achieve, for many of the same reasons as optical switching. Devices to achieve optical gain such as the microchannel spatial light modulator[31] are expensive and have high energy consumption relative to equivalent electronic devices.

To summarize, we believe it makes sense, for both practical and fundamental reasons, to implement the feedback loop electronically (including the non-linear functions required).

The strawman architecture has been summarized in Figure 22. This architecture contains all the features required for realization of a general purpose network: implementation of arbitrary multilayer networks, feedback, backpropagation for learning, and very large interconnect capacity.

4.4 Photon Budget and Material Requirements

This section presents an analysis which shows the relationship between SHB material selection, photon counting efficiencies, signal to noise, the type of hologram used for storage, and system capacity. This problem is multi-dimensional in more ways than one. The details of the problem will be worked through sufficiently to define a region of interesting material parameters and how they relate to system performance.

The problem to be considered here is a first cut at the factors which will define the fundamental and practical operating limits of a 4D neural net computer based on spectral hole burning (SHB) materials. The principal objective is to define the materials and fundamental details of the neural net system which are required for reliable operation. To simplify the discussion we shall concentrate on two systems for examination 1) a small scale, or demonstration, system which is aimed at simply exhibiting simple and perhaps slow 4D neural net calculation operations, and 2) a large scale (large in capacity, not physical size), high speed version which will be developed in the long term. The discussion will show the clear relationship between material properties and the functional performance of the neural net. In order to assist in the discussion the material and system parameters of importance are specified in Table II.

4.4.1 System Specifications

The large scale system will be defined as:

1. SLM and input data arrays are 1000 by 1000.
2. Cycle time of neural net: 1 msec pulsed, 30 msec continuous.
3. Power limits of laser: 100 mW.

The large scale system should be interpreted in light of the following relationships. Data arrays of 1000 by 1000 imply the storage of 10^6 holograms, each containing 10^6 bits. Thus the storage capacity of the system is 10^{12} bits. The effective operation rate of the system is 10^{12} operations in 30 milliseconds, or about 3×10^{13} operations/second.

Table II. Material Model Parameters

C_p	Specific Heat of SHB material.
σ_T	Thermal conductivity of SHB material.
n_p	Molecules per recorded pixel.
σ	Molecular absorption cross section.
QE	Quantum efficiency of the SHB material.
η_d	Detector quantum efficiency.
N_p	Number of photons incident on a detector pixel.
N	Number of pixels in a row or column of the input or output arrays.
N_n	Detector noise equivalence in photons/pixel.
P	Probability of error in an array of output data.
p_i	Probability of an error in a single pixel of output data.
SNR	Signal to noise ratio.
PPB	Photon/pixel budget.
η	Hologram efficiency.
Φ_r	Required photon flux for reading.
Φ_w	Required photon flux for writing.
f	Fraction of light transmitted by chromatic filter over detector.
$N.A.$	Numerical Aperture.
S_p	Scattered number of photons/pixel.
δ	Angular selectivity of a recorded hologram.
λ	Wavelength of light.
n_o	Refractive index of holographic material.
T	Thickness of holographic material.
θ	Angle of incidence of illuminating beams used for holograms.
γ	Homogeneous linewidth at half maximum.
ω	Frequency of the laser.
ω_o	Frequency of the homogeneous line center.
$O.D.$	Optical density of the SHB material.
ρ_m	Molecular density of the photochemical.
α	Absorption coefficient of the SHB material.
α_1	Modulated absorption coefficient of the SHB material.
α_o	Average absorption coefficient of the SHB material.
n_1	Modulated component of the real refractive index.
R_e	Allowed number of read operations before erasure.

4.4.2 Signal to Noise Ratio

It is difficult to define the SNR for a neural net because the fault level in the system is interdependent with the algorithm used. In order to provide some guidance, however, the following is suggested as a formalism for estimation of the propagation of errors. For a 4D neural net system the output plane is a square array of N by N pixels. On a single pass through the net a single "answer" is required. The "answer" is a collection of output pixels being turned "on" in a unique manner which identifies a result (or collection of results).

From a consideration of random errors, it can be suggested that the probability of a particular

pixel being incorrectly identified (due to photon counting errors, not due to the calculation issues associated with the neural net algorithms, etc.) is p_i. The probability that any single pixel among N^2 pixels is incorrectly identified is then simply $N^2 p_i$ (for small p_i). If we require that the complete data array which is provided by the neural net on a single pass have a probability of error of P then the error level allowed for a single pixel is simply

$$p_i \cong \frac{P}{N^2}. \tag{14}$$

In the detector electronics, it must be assumed that a threshold is to be set which will be half way between the average noise level and the average signal level. However we shall assume that the noise is significantly smaller than the signal and the half way point is simply the signal strength divided by two. Therefore the probability that a particular single pixel will provide an erroneous answer can simply be related through Gaussian statistics as

$$p_i = 2[1 - erf(\mathrm{SNR}/2)]. \tag{15}$$

Equation (15) can be readily approximated by a series expansion and when combined with equation (14) will provide an explicit relationship between the probability of error of the system on a single pass and the signal to noise ratio.

$$P = N^2 \frac{2e^{x^2}}{\sqrt{\pi}x}\left(1 - \frac{1}{2x^2} + \frac{1 \times 3}{(2x^2)^2} - \frac{1 \times 3 \times 5}{(2x^2)^3} + \ldots\right) \tag{16}$$

where $x = \mathrm{SNR}/2$. This formula quickly converges for reasonable values of SNR and representative results are given in Table III. The net conclusion which can be drawn from the results presented in this table are that a desirable SNR for the demonstration system would probably require a pixel level signal to noise of between 5 and 10, while the large scale system should have between 10 and 15. We can readily see that the reliability of the system is a strong function of the pixel level SNR, and that beyond a SNR of 15 it would seem that little is to be gained in realistic reliability. For the sake of simplicity, we shall set the required SNR as being 10 for both systems.

Table III. Pixel SNR Relation to System Probability of Error

SNR	N^2	P
5	10^2	8.0×10^{-2}
10	10^2	3.0×10^{-10}
15	10^2	5.6×10^{-24}
5	10^6	1.0
10	10^6	3.0×10^{-6}
15	10^6	5.6×10^{-20}

This defines the required SNR for the entire system, which include "random" errors from all sources. If the error budget is composed of several factors, it may be reasonable to require that the contribution of any single error source must be a fraction of the total error. For this reason, we shall set a reasonable limit to the photon detection budget at a SNR of 15.

Since the strength of the stored image is intimately related to the SNR, a requirement of the system is all of the stored images have the strength required. If they do not, then the results would either require a larger SNR per pixel, or they would not be quantitatively correct. The most direct way to address this issue is to maintain a consistency of illumination during reading and writing. This can be done if the stored images all contain a "reference block" which can be used to monitor recording level automatically. This recording block should be larger than a regular pixel, allowing for greater statistical certainty to be attached to the measurement. It may even need to be a separate detector.

4.4.3 Photon Budget and Selection of Detector

From the above discussion it was concluded that the SNR at the detector plane due to photon measurement issues must be about 15. If the limitation were simply due to photon counting statistics in a noiseless detector, the required number of detected photons/pixel in a given cycle of the neural net would be 225. The performance of realistic and presently available detector arrays[32] is shown in Figure 23, and Table IV. The curves in Figure 23 can be readily calculated from a simple formula relating the SNR to the detector noise (N_n), photon collection efficiency (η_d) and the randomness of the photon counting statistics (number of photons = N_p).

$$\text{SNR} = \frac{\eta_d N_p}{\sqrt{\eta_d N_p + N_n^2}} \tag{17}$$

From the curves in Figure 23 we can see that the best detector available would require about 500 photons/pixel with optimal integration time, while the "worst" selection would require about 3×10^4 photons/ pixel. The difference between these performance requirements lies largely in the determination of data rates and cooling of the detectors. For the sake of compromise, we shall set the number of photons required to provide an SNR of 15 as 1000 photons/pixel. Should the photon/pixel budget (PPB) need to be reduced, the detector can be cooled and readout can be slowed down, but this will only buy a factor of 2 in the number required.

There are many neural net applications where the output signal is filtered by a sigmoidal function which has the effect of limiting the dynamic range requirement significantly. Under those circumstances, 8 or 12 bit precision is probably more than adequate.

4.4.4 Photon Budget and the Laser Requirements

With this requirement for the number of photons/pixel established, one may now assess the reading requirements of the neural net as being the PPB times the number of pixels (N) which are required to be illuminated for a single wavelength of illumination by the laser. (This corresponds to the illumination of a single column in the detector array.) Therefore the number of photons in the detector plane may be required to be as large as $N \times \text{PPB}$. The number of photons which must be incident upon the SHB material to provide the required signal is now a function of the

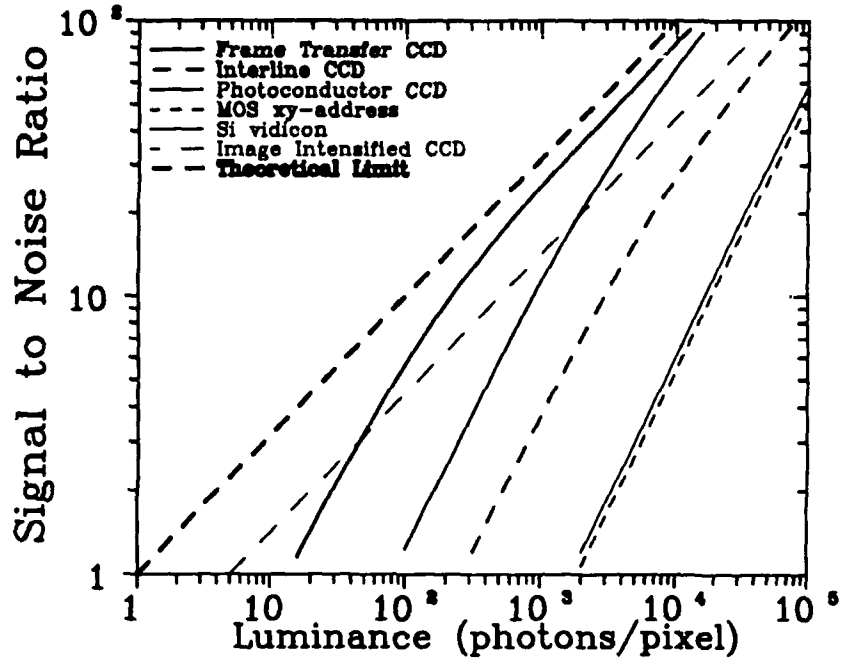

Figure 23. Photon-limited signal to noise ratio calculated using equation (4).

diffraction efficiency η of each recorded hologram. The required photon flux summed over all the wavelengths required for reading (Φ_r) is then

$$\Phi_r = N^2 \, \mathrm{PPB}/\eta. \tag{18}$$

The diffraction efficiency of a hologram (η) is given by Kogelnick's adaptation of the coupled wave theory[19] as

$$\eta = [\sinh^2(\alpha_1 d/4\cos\theta) + \sin^2(\pi n_1 d/\lambda\cos\theta)]e^{-\alpha_o d/\cos\theta}. \tag{19}$$

The above equation describes the composite hologram efficiency when both phase and absorption effects are contributing. For holograms of modest efficiency (less than 1 percent) the hologram efficiency is proportional to the square of the index modulation (real or imaginary). If a minimum hologram efficiency is specified, the index modulation required for each (α_1, or n_1) can be readily calculated. If the maximum index modulation values permitted (the dynamic range of the material) is known then the number of holograms which can be stored at a single frequency can quickly estimated. (So far, the literature on SHB materials primarily reports diffraction efficiencies on the order of 10^{-4}, while the theoretical efficiency for an absorptive hologram can be as high as 3.7×10^{-2}, and for a phase hologram it can be 1.0.) If a minimum hologram efficiency of 10^{-5} were required and the maximum hologram efficiency of the material were 3.7×10^{-2}, one could store as many as 60 holograms at the same frequency. With phase holograms, the number can be much larger.

Table IV. Characteristics of Modern Electronic Image Sensors.[32]

Sensor Type	Example	Application	Number of Pixels	Image Area (mm^2)	Sensor Noise (e/pixel)	Quantum Efficiency
Self-Scanned silicon sensors	Frame-Transfer CCD	Astronomy	2048× 2048	55×55	9 (slow scan)	0.70 (thinned)
	Interline CCD	High-def TV	1280× 980	12.7× 9.5	36	0.14
	Photo-conductor over CCD	High def TV	1920× 1036	14.0× 7.8	52	0.65
	MOS xy-address	Color camcorder	649× 491	8.6× 6.5	745	0.40
Photo-conductive camera tubes	Saticon	High-def TV	1050000 (at 20 MHz)	12.7× 9.5	1500	0.90
	Si vidicon	Low light levels	210000 (at 4 MHz)			
Image intensifiers	Image-intensified CCD	Scientific	684×576	18mm (diagonal)	High gain overrides	0.20
	Photon-Counting Imager	Astronomy	512×512 digital store	Position-sensitive detector	noise	0.20

4.4.5 Material Requirements and the Photon Budget

During this task, we examined the requirements placed on the interconnect recording medium by the required signal to noise, allowable medium heating, required medium sensitivity, and other limits. We found that some of these requirements would limit the performance of our architecture, while others were irrelevant. This analysis indicated that existing materials can satisfy all the requirements for recording and using extremely large numbers of interconnects in a 4D holographic configuration.

Heating of the SHB Material. What is the power deposition rate permitted? For SHB material, maintained at 4 K, we might allow a temperature rise of 1 K before it impacts performance. A larger temperature rise might effectively broaden the homogeneous line width, reducing hologram efficiency and introducing crosstalk. This "power broadening" effect is fundamentally related to the thermal characteristics of the SHB material. The specific heat of a typical plastic material at low temperature (such as polystyrene) is about 4 mJ/g-K[33]. From typical organic material thermal conductivity values for materials such as polyethylene [34] we

can estimate a value of about 1.3 mW/cm-K. For a 1 cm cube, a crude estimate of the heat loss from the center of such a cube would allow for an input of up to 3 mW without serious heating problems.

The required hologram efficiency is directly traceable to the heating limits of the SHB material if we assume that the vast majority of the photon flux used for hologram reading is absorbed by the SHB material and turned into heat. At a continuous neural net cycle time of 1 per second the hologram efficiency must be 3.7×10^{-7} or greater. In burst mode, the net would be allowed 3 complete cycles (at 1 cycle per msec) before slowing down to the steady state. By increasing the efficiency of the holograms, both the continuous read rate and the burst mode capacity increase proportionately. To achieve a reasonable rate of neural net operation rate, a hologram efficiency of 10^{-5} would be indicated, which would then permit a continuous mode operation rate of about 30 Hz and a burst capacity of about 300 cycles.

Heating: Hologram Efficiency $> 10^{-5}$.

In this section we shall consider the issues specific to the storage of multiple holograms in SHB materials and the efficient read out of those holograms with tolerable levels of erasure occurring during the reading process. The main consideration will be a determination of performance limits in terms of known SHB materials and a discussion of whether absorption or phase hologram storage is required.

Storage of Holograms as a Function of Frequency. The basic structure of the proposed 4D neural net dictates that the holograms be divided into at least as many frequency groups as there are columns in the SLM. This permits definition of the frequency dimension during storage and readout. The number of holograms within a single frequency group (i. e. assigned to a single column) is then simply the number of rows in the SLM. For our large scale system this may be anticipated to be 1000 holograms. This would imply that 1000 holograms might be stored at a single wavelength. Theoretically, an absorption transmission hologram is limited to 3.7 percent. If broken into 1000 equal holograms, this permits an efficiency of 3.7×10^{-8} for each, which may prove to be a point of concern from simple scattering effects and from power requirements for the laser as well as heating of the SHB material.

The scattering issue can be dealt with adequately either by the use of higher efficiency holograms or by the implementation of a chromatic filter in front of the detector.

The anticipated scatter may be expected to be of the order of 0.1 percent even for a well designed system. If this scatter is isotropic, and we have an optical system with an N.A. of 0.15, the fraction of the photon flux used in reading which will be directed toward the detector plane is about 2×10^{-6}. The scatter/pixel (S_p) is then given by

$$S_p = \frac{2 \times 10^{-6} N^2 \mathrm{PPB}}{\eta N^2}. \tag{20}$$

An option exists which can allow storage of absorption holograms at efficiencies of higher than 3×10^{-8}. The approach would be to create several frequencies for storage within a single frequency range assigned to a column. This would permit fewer holograms to be stored at each frequency, thereby permitting each to have a higher efficiency. For example, if 32 holograms are stored in 32 separate frequencies within each "color column", the efficiencies of each hologram can be raised to 3×10^{-5}. This eliminates the scattering issue but increases the number of frequencies at which holograms are stored by a factor of 32.

Phase hologram storage may have a significantly larger dynamic range permitting a significant reduction in the number of frequencies within each channel. The use of several frequencies for storage within a single column can again be used to increase the hologram efficiency.

The previous section argued for the use of hologram efficiencies greater than 10^{-5} in order to prevent excessive heating of the SHB material. If these "high efficiencies" are used the color filter can effectively be eliminated. Under these conditions the scattered photon flux is now only 300 photons/pixel. This scattering rate is acceptable but shows that care must be exercised in applying proper optical coatings.

Crosstalk Between Holograms. If, in the process of reading holograms, the light is partially scattered by images which were stored and are being read out unintentionally, then they can contribute to false signals, which can effectively be considered as part of the SNR budget. Crosstalk can occur in two fundamental ways.

Crosstalk Due to Angular Resolution. Two holograms which are stored at the same wavelength using reference beams which are closely spaced angularly can have an efficiency overlap. This comes directly out of the basic theory developed by Kogelnik[19]. From his analysis we can quickly see that the storage limits are determined largely by the thickness (T) of the material used. This militates toward using materials which are 0.5 to 1 cm thick. This would provide an angular selectivity at which crosstalk can be reduced to less than 1 part in 20 for all holograms except very high efficiency (near 100 percent) phase holograms. These high efficiency holograms are unlikely to be necessary for high performance requirements and so they will not be considered seriously here. The angular selectivity (δ) for very low crosstalk can be estimated as

$$\delta = \frac{\lambda}{2n_0 T \sin\theta}. \tag{21}$$

If the angle of incidence is 10 degrees, and the wavelength is 0.7 μm, the angular selectivity for a 0.5 cm thick hologram would be 3×10^{-4}. For an optical system having a numerical aperture of about 0.15, this would allow one to cleanly resolve 1000 elements within the field of view. This defines the size of the SLM as being directly related to the thickness of the SHB material.

Crosstalk Due to Frequency Spacing. The crosstalk between holograms which are at different wavelengths but the same angle (same row of input) also needs to be considered. Kogelnik's theory provides some wavelength selectivity, however this is quite inadequate. The greater selectivity is provided by the SHB material itself through consideration of the Kramers-Kronig relation. The principal point of interest is seen in Figure 24 where one notes that a modulation in the absorption as a function of wavelength (or frequency) is directly related to an accompanying change in the real part of the refractive index. Both parts of the complex refractive index can contribute to the strength of the hologram. The key element to be noted here is that the absorption modulation at ω_o has an effective "range" in frequency space which can interfere with holograms which might be located nearby (in frequency). This effect will introduce crosstalk, and will define a limit to the ability to "pack in" information in frequency space.

For simple modulations of the absorption, as seen in typical SHB structures, the effective strength of the hologram will fall off with frequency according to a simple formula[15] (for low efficiency holograms)

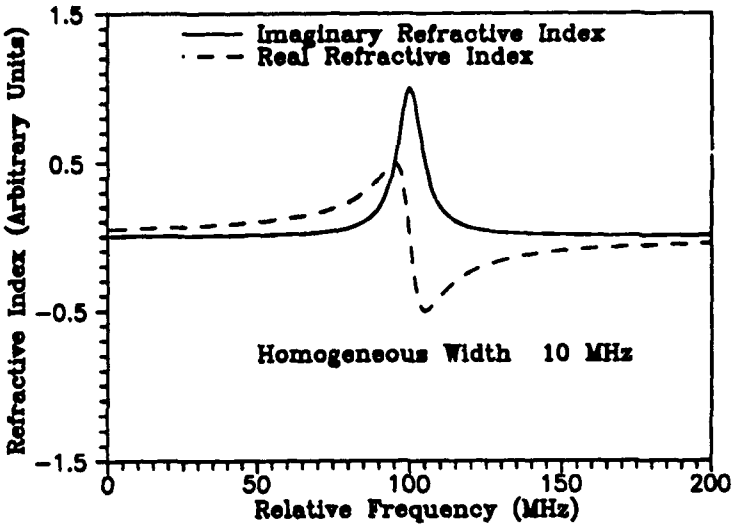

Figure 24. Real and imaginary components of the refractive index for a single damped oscillator. Note that the real part has an effective range that extends well beyond that of the imaginary component.

$$\eta(\omega) = C\frac{(\gamma/2)^2}{(\omega_o - \omega)^2 + (\gamma/2)^2}. \tag{22}$$

In the above, C is simply a constant which describes the background absorption, hole depth, and geometrical properties of the hologram, while γ is the spectral linewidth of the SHB material. (It is assumed here that the width of the absorption profile which was created was as narrow as was permitted by the material, and not limited by power broadening, linewidth of the laser, or other effects.) As discussed above, crosstalk between adjacent (in frequency) holograms should be considered a source of noise, and the SNR be kept above the required level of 15. Since noise can occur from holograms stored on either side (in frequency space) of the selected frequency, the actual SNR limit is doubled to 30. Since hologram storage is occurring in the 2 dimensional plane of frequency and reference beam angle one is required to enhance the spacing further by roughly $\sqrt{2}$ which then places the required SNR at 43. From equation (22) this would require that the holograms be spaced greater than 6.5 γ apart.

When pushed to the limit, many holograms can be stored within a frequency range defined by a homogeneous linewidth. This can be seen through several examples. If the number of holograms stored at a single frequency is 1000, the spacing required between frequencies is 6.5 times the homogeneous linewidth. For the storage of 1000 columns of information, this requires that the inhomogeneous linewidth be 6500 times the homogeneous linewidth. This is readily achievable for virtually all interesting SHB materials. As the number of holograms stored at each frequency is reduced, the width of the inhomogeneous line must increase. If 32 holograms are stored at a single frequency, the inhomogeneous linewidth is now required to be 208,000 times the homogeneous linewidth.

Such SHB materials are known to exist. In fact, one can immediately extract a necessary homogeneous linewidth if the inhomogeneous line width is known. For materials with an inhomogeneous linewidth of 9 THz, the homogeneous linewidth must be 45 MHz for storage of 32

holograms at each frequency. These requirements can be relaxed somewhat if more than one SHB species is present in the host so that a larger frequency range is available or if more than 32 holograms can be stored at each frequency. The hologram efficiency limit of 10^{-5} would permit storage of 60 holograms at each frequency. The required homogeneous linewidth is now only 90 MHz. The laser line width must be comparable to the homogeneous line or narrower.

Homogeneous linewidth $< 90\ MHz$.

Molecular Densities. To achieve the highest possible efficiency holograms as well as permit reliable storage of detailed images, one faces some limitations in the molecular densities allowed. As it turns out, this also relates directly to some of the fundamental properties of the dopant molecules and the solvent materials.

For images stored as absorption transmission holograms, maximum efficiency is achieved when the optical density (O.D.) is approximately 1. This places a limit on the molecular density (ρ_m) of the absorbing species for which the absorption cross section (σ) is fixed.

$$\rho_m = \frac{(\text{doping level})(\text{density of host})}{(\text{molecular wt. of solute})}(\text{Avogadro's Number}). \tag{23}$$

$$O.D. = \frac{\alpha}{2.303} = \frac{\rho_m T \sigma}{2.303}. \tag{24}$$

With the thickness (T) set at 0.5 cm, and $O.D.$ set at 1, (for the large scale 4D neural net outlined above) we find that the absorption cross section and molecular densities are directly related (in units of cm^2) as

$$\sigma = \frac{4.606}{\rho_m}. \tag{25}$$

If our target is to achieve storage capacities of 10^{12} bits/cm^3, the molecular density must exceed this by several orders of magnitude in order to provide reliable data storage and retrieval. A first cut at this can be provided by demanding that the fundamental data storage have an SNR of 20. This then allows us to define a number of molecules per pixel (n_p) needed to properly define the situation. On fundamental counting statistics arguments, this would require 400 molecules/pixel (minimum). This relates directly to the molecular density as 8×10^{14} molecules/cm^3. For an inhomogeneous linewidth of 9 THz and a homogeneous width of 90 MHz, this translates into a minimum of 8×10^9 molecules/cm^3 within each homogeneous linewidth. The upper limit on the absorption cross section is then set at 5×10^{-10} cm^2 per molecule. For phase hologram storage, the absorption cross section could be as much as 100 times larger because reading and writing occurs in the bleached frequency channel.

Molecules/pixel Requirements (Absorption Hologram): Cross Section $< 5 \times 10^{-10} cm^2$.

Molecules/pixel Requirements (Phase Hologram): Cross Section $< 5 \times 10^{-8} cm^2$.

From the other extreme, the maximum molecular density is reached when the spacing between molecules causes the molecules to be coupled by long range interactions, thereby causing the homogeneous linewidths to broaden. This limit is reached with a molecular density of about 2.5×10^{20} molecules/cm^3. Within each homogeneous linewidth, the maximum molecular density is then 2.5×10^{15} molecules/cm^3. This sets a lower limit on the allowed absorption cross section of 2×10^{-15} cm^2. For high density phase hologram storage the limit is 2×10^{-13} cm^2.

Molecular Density Limits (Absorption Hologram): Cross Section $> 2 \times 10^{-15}$cm^2.

Molecular Density Limits (Phase Hologram): Cross Section $> 2 \times 10^{-13}$cm^2.

Power Requirements for Writing. The efficient writing of holograms is fundamentally limited by the number of molecules required per stored pixel and the quantum efficiency of the molecule to undergo the photochemical process. In a hologram containing N^2 pixels, with n_p molecules/pixel, and a quantum efficiency for bleaching of a molecule of QE, the number of photons needed to write a hologram (Φ_w) is

$$\Phi_w = \frac{n_p N^2}{QE}. \tag{26}$$

With a data recording rate of 1 GHz, 400 molecules/pixel and $N = 1000$, the minimum quantum efficiency allowed is 10^{-7}. As the molecular cross section decreases and the number of molecules required per stored pixel increases, the required quantum efficiency increases proportionately. This limit is the same whether absorption or phase hologram storage is assumed, so long as the optical density at the recording frequency is held at 1.

$$QE > \frac{5 \times 10^{-17}}{\text{molecular cross section}} \tag{27}$$

Another phenomenon has been noted which can limit the hologram writing rate. For phthalocyanine (H_2Pc) a "bottleneck" has been determined[14] which can fundamentally limit the writing speed. The molecule is changed photochemically through a complex 4 level process (see Figure 25). Upon excitation, the molecule quickly decays from the initial excited state to a long lived (350 μsec) metastable state. From the metastable state, the decay branches to the chemically changed state (about 1 percent) or reverts back to the initial ground state. Under high photon flux conditions, all the molecules can be populated up to the metastable state, not permitting any further absorption until decay occurs. If high hologram efficiencies are required, one may need to be working with a molecular population much greater than that associated with the storage of a single hologram, or the time to write the hologram must be greater than the lifetime of the metastable state. In practice, for large scale systems, this will not be a serious concern, because of the storage density and molecular densities of the material.

Reading versus Erasure. In a previous section it was concluded that reliable reading of information required photon fluxes (PPB) of about 1500 photons/pixel. (This quantity is related to the reading of a column of pixels which identify a single hologram.) In order to be read out, we shall hypothesize the "worst-case" scenario where all the photons for the column of pixels in the output plane are incident at a single wavelength. The photon flux required at each wavelength is then given directly by equation (18). It was also concluded that hologram efficiency played a significant role in the flux required to read it.

For a practical system, there must be a clear differentiation between the reading and writing operations to the level where the information may be read out several times without significant erasure. On this basis one needs to define a minimum number of read operations allowed before erasure occurs (R_e). An approximate criterion for stable operation of the neural net is then defined to be that the number of photons required for reading, times the number of read

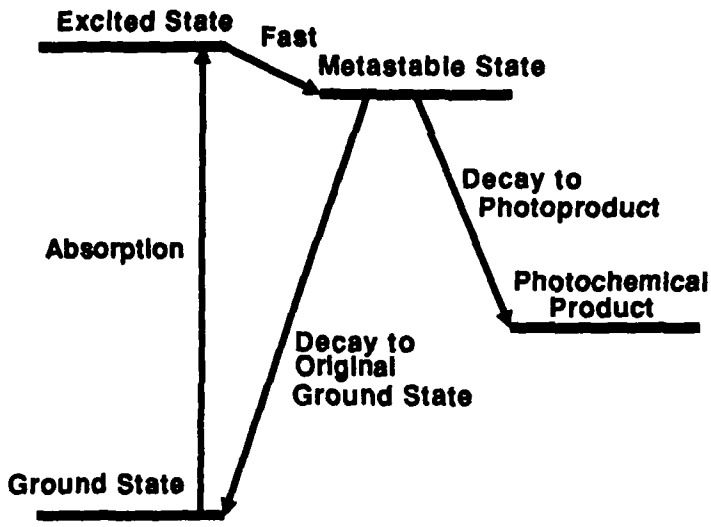

Figure 25. Diagram of the molecular energy levels for H_2Pc showing how the direct absorption leads to the population of a long lived (350 μsec) metastable state before decaying either back to the original ground state or toward the photochemical product state.

operations allowed, be less than the number of photons required to create the hologram. (This assumes that the SHB medium is being utilized to its fullest in the storage of information.)

$$R_e \, \Phi_r < \Phi_w$$

$$R_e \frac{N \text{ PPB}}{\eta} < \frac{n_p N^2}{QE} \tag{28}$$

This now defines a requirement on the SHB material which relates quantum efficiency to hologram efficiency.

To see how this relates to the selection of real materials, in order to permit a minimum of one read operation before erasure, and for 400 molecules/stored pixel, the QE must be less than 2.7×10^{-3}. As the absorption cross section is reduced (and the number of molecules/pixel is increased) the upper limit on QE proportionately increases.

Since the lower limit on QE is a parallel limit with absorption cross section, the allowed number of reads without erasure can be increased significantly by reducing the QE toward that lower limit. In doing so we find that the upper limit on reads without erasure is 27,000 which would seem to be quite an acceptable limit.

A simple way to increase the allowed number of reads is to increase the total molecular base further, so that the initial hologram storage only accounts for a fraction of all the molecules available. This cannot be done for absorption holograms, because the hologram efficiency is intimately connected to the molecular density and absorption cross-section. However, the phase hologram approach allows significantly expanded storage capacity. If the total molecular capacity

were 100 times greater for a phase hologram approach, the upper limit on QE could be raised by 10^2 and the allowed number of reads before erasure could approach 2.7×10^6.

For this reason, if many read operations without erasure are required, the phase hologram approach can be considered critical to achieving the necessary high performance.

Overall Material Boundaries and Comparison with Bit-Oriented Storage. The above considerations serve to provide boundary conditions to the fundamental materials selection process behind the SHB approach to 4D neural nets. These boundary conditions are presented in Figure 4, following the format of Moerner[18], with the bit-oriented storage system results seen in Figure 5 for comparison.

1. The upper boundary on the hologram approach is set by the read/erasure limit which relates to one successful read before erasure. The phase hologram storage approach could raise this limit by a factor of 100 or more. There is an ultimate limit to the allowed QE which was referred to in the above reference related to molecular issues described as "photochemical broadening."
2. The lower boundary on the absorption hologram approach is set by the power dissipation requirements during writing. This same boundary holds for the phase hologram storage approach. (In a bit-oriented storage scheme there is a similar limit caused by the inability to rapidly bleach a large ensemble of photochemical molecules without broadening the effective width of the spectral hole.)
3. The boundary on absorption cross section is determined by the molecular storage limits and optical density requirements of the holograms and is 5×10^{-10} cm^2/molecule for the absorption hologram, and about 100 times greater for the phase hologram.
4. There can be anticipated to be some limitations on molecular densities due to nearest neighbor effects and limitations on the spectral hole width. These considerations place a lower boundary on absorption cross section of about 10^{-17} cm^2.

If phase holograms are used for storage, the number of reads without erasure is greatly increased. The heat dissipation problem might be somewhat reduced if the absorption of the medium can be reduced, This might permit a higher continuous cycle rate.

It can be seen in Figure 26 that a suitably large material property region is available for phase hologram storage, while the absorption hologram approach provides a significantly smaller region where system performance is acceptable. By comparison, Moerner's results[18] are shown in Figure 27 for bit-oriented storage. We readily find that the region of material property space which provides acceptable performance is much larger for hologram storage, and includes some already studied materials. This difference is largely due to the manner of data storage used which allows for the recording of an entire array of data (10^6 pixels) in a single hologram, while bit-oriented recording requires one bit at a time recording. The net result is that the power densities required for efficient data rates in bit-oriented storage have severe thermal effects, which are minimized in volume holographic storage.

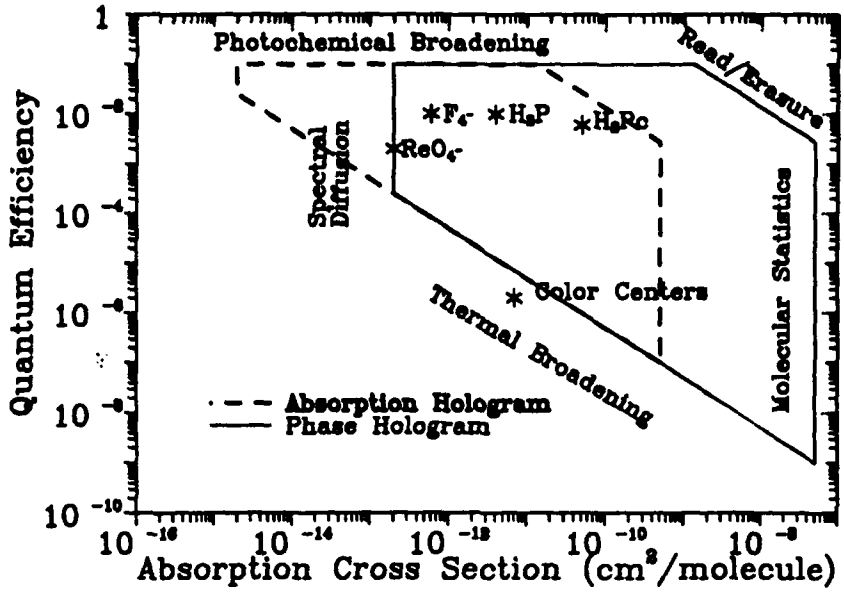

Figure 26. Allowed region of quantum efficiency and absorption cross section for a holographic 4D neural net application with the capabilities outlined above.

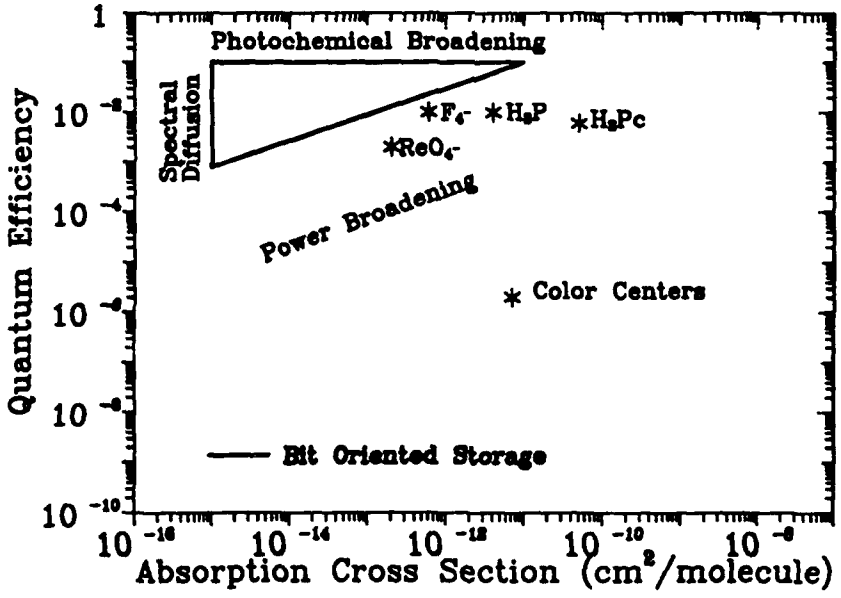

Figure 27. Allowed region of quantum efficiency and absorption cross section for a bit-oriented memory application using SHB materials (taken from reference 18).

4.4.6 Photon Budget Conclusions

The fundamental photon limiting statistics can lead to the definition of some technical boundaries for a realistic large scale system. This leads to the summary of system specifications outlined in Table V. The boundaries are more stringent for absorption hologram storage than for phase hologram storage. In general these boundaries expand proportionately as the system performance requirements are relaxed. These boundaries are of little fundamental significance in the demonstration of a small scale 4D neural net, but they can become a significant issue when large scale systems are designed for certain applications. It can be inferred that system performance may be hampered by the use of absorption holograms for the large scale system. By comparison, the use of phase holograms may provide sufficient latitude to make such a large scale system feasible.

Table V. System Requirements Summary

The large scale system will be defined as:	
Data Arrays	1000 by 1000
Cycle Time	1 msec pulsed, 30 msec continuous
Laser Power	10 mW
Reference Block Required	
Cooled Detector	
12 Bit A to D converter	
SLM Uniformity	$\pm$10 percent
SLM Contrast	10
Cryostat Cooling Capacity	3mW
Laser Linewidth*	90 MHz
Reads Before Erasure*	2.7×10^4 (absorption hologram)
Reads Before Erasure*	2.7×10^6 (phase hologram)

*This can be increased by use of multiple SHB solute materials being dissolved in the same host.

4.5 High End Optical System Analysis

The high end system design is far more compact than the experimental system for a number of reasons. To determine the scope of a possible design, however, several assumptions are required concerning technological developments. These developments are not considered to be physically unreasonable, but they would be presently quite costly to implement in an experimental design and have been avoided in the analysis of the experimental system. Under the assumptions detailed below, as analysis is presented which shows the physical size of a 4D neural net system.

The layout of the optical system for the final high end system is similar to the experimental system only in the detailed aspects associated with the cryostat and detector optics. The beam

dispersion, beam expansion, SLM, and reduction optics can be significantly simplified by assuming that an SLM will be developed with pixel dimensions in the range of 10 to 15 μm per pixel, with contrast capabilities in the range of 100 or better. This assumption is not unreasonable. It is already being addressed through active SLM development programs (see Figure 28).

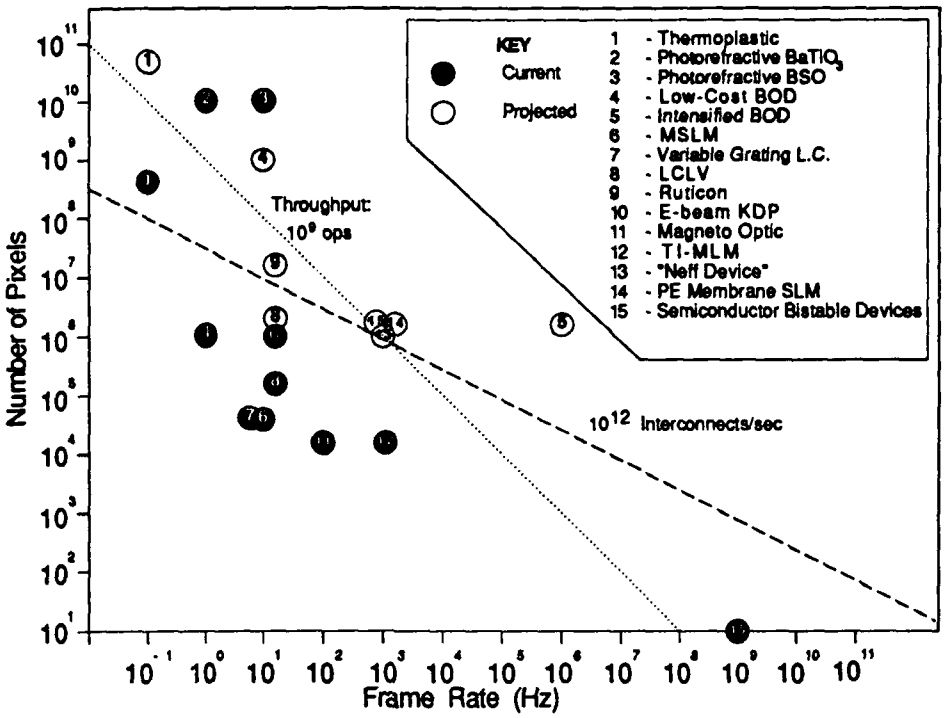

Figure 28. Current and projected capabilities of spatial light modulators.

An extra assumption which would be extremely desirable would be the development of a compact solid state frequency agile laser (FAL). This last assumption could make the total system size then be limited primarily by the combination of cryostat, optics, and light source.

System Specifics. There is an effective minimum size for the proposed 4D system which is largely set by the physical size of the cryostat. The size of the cryostat makes consideration of very small optical systems with small components and a low capacity system of little interest. Even a compact cryostat unit might be expected to require a physical size of a cube 15 cm on a side, or more. For this reason alone we shall set the minimum size of the 4D neural net at this dimension. Growth beyond this volume we shall attribute to optical requirements.

At the interconnect capacity of 10^{12} the SLM need only take on the dimensions of a 1 to 1.5 cm square. The system requires no image reduction, and the numerical aperture is limited by geometric and holographic arguments to be about 0.07 or less. The allowed angle of incidence of the beams (to permit reasonable holographic fringe spacing) is also similarly limited. These considerations will limit the number of pixels in an SLM plane to not more than 1000 per dimension.

The optical requirements on the 4D system are not significant, as the SLM is compact and beam dispersion may not be required (see Figure 29). The beam expansion can take place in a distance of roughly 5 cm. The beam splitter path can be made conveniently short (a few cm).

The beam path from the SLM to the SHB would be no more than that seen in the experimental system (12 cm) and the path to the CCD arrays would be identical (12 cm). The total beam path would then not need to exceed 35 cm. With modest folding of the optics, it can be seen that the entire optical system (exclusive of the laser) could be contained within a cube which is already defined by the cryostat requirements. If the laser were of similar size to the cryostat, the overall system would be of a dimension which could be easily held in one hand. If the laser could be reduced to a tuneable laser diode concept, the laser might add very little to the complete system size.

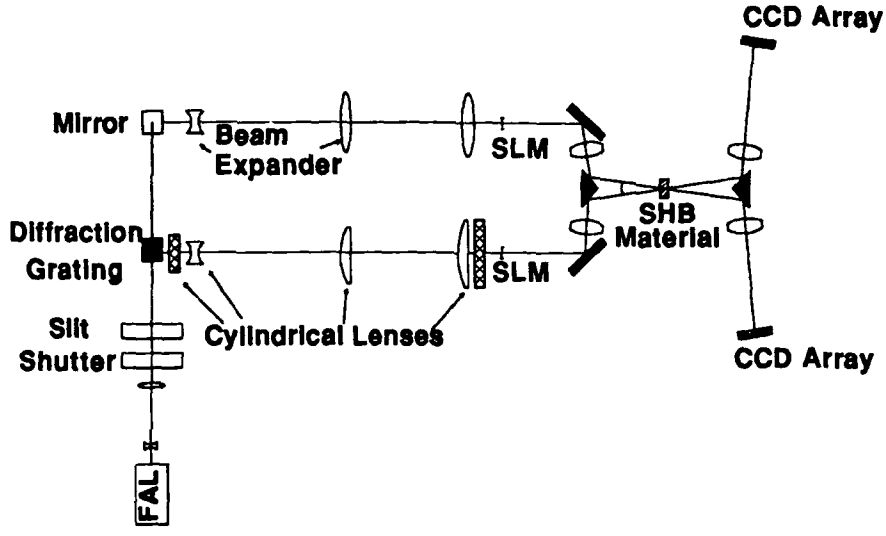

Figure 29. Optical details of an advanced compact 4D neural net computer.

4.6 Cryostat Requirements

From the analysis provided above, the power utilization of the system can be anticipated to be quite low. The properties of the SHB medium will be best maintained when the incident light level is in the range of a few milliwatts. Furthermore, the overall design of the high end system is inherently compact. This permits the cryostat requirements to be reduced to a very acceptable level where the heat load of the SHB material is of only modest concern.

Commercial systems are presently available which are simple closed cycle refrigerators and of modest size (even in their present state of development). For ground oased applications, such cryostats could provide cooling capacity for as many as 100 of our proposed large scale neural nets. With some engineering development, these cryostats might also be reduced in size and power requirements to make them more convenient for a wide variety of users.

For space-based applications, the low heat dissipation and compact design again permits ready application of known technical approaches to permit operation for a year or more in

space with only modest requirements put on weight and size, and virtually no impact on power requirements for operation. The use of solid-cryogen system, which have been well tried and developed, should provide a very acceptable approach.

COMMERCIALLY AVAILABLE REFRIGERATOR

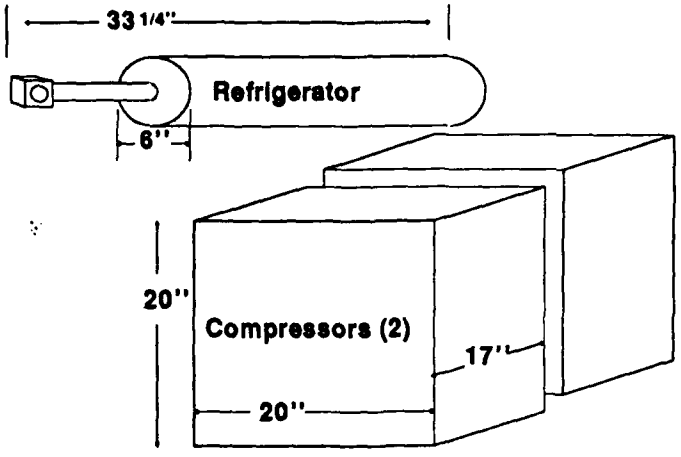

Power Required: 3 kW.
Ultimate Temperature: 3.6 K
Refrigeration Capacity: 1W at 4.2K

Figure 30. Example of a presently available commercial refrigerator system which can readily achieve the cryogenic conditions required, and has sufficient capacity for many neural nets of the size proposed.

SOLID-CRYOGEN-STORAGE COOLING SYSTEM

(Conceptual: Based on Similar Space Qualified Systems)

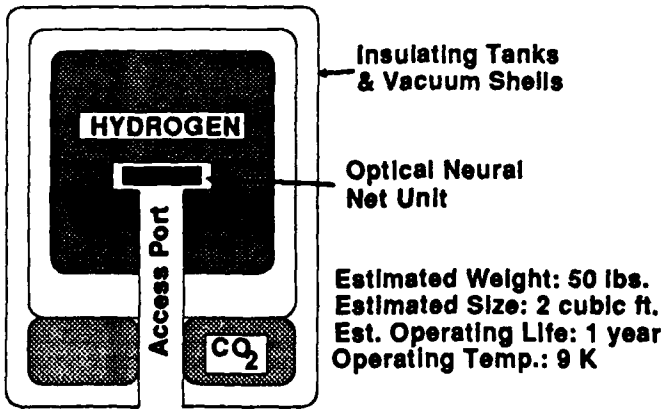

Figure 31. Conceptual drawing of a space qualified solid-cryogen-storage cooling system. Such systems have been built and used in space based applications where cooling is required for a year or more.

5 Spatial Light Modulator Requirements

This section summarizes the results of Tasks 2 of our Phase I Statement of Work, Determination of Spatial Light Modulator Requirements.

The requirements for the spatial light modulator depend on the architecture of the system. These requirements include the number of pixels (space-bandwidth product), the update time of the network, the pixel size, independence of amplitude and phase modulation, and the contrast requirements.

5.1 Photon Budget and the Spatial Light Modulator (SLM)

The capability of the SLM plays into the SNR through consideration of the contrast of the pixels. If the contrast of a given pixel is limited (i.e. 10:1 or 100:1) then this can have an influence upon the total photon flux requirements. For an SLM having a contrast of 10:1, the net effect will be to bias the noise upward but not really increase the magnitude of the noise itself. This can be readily compensated by increasing the signal magnitude requirement (PPB) by about 10 percent for a contrast of 10, or 1 percent for a contrast of 100.

A different effect caused by the SLM can occur if the transmission of the SLM is not uniform in the clear or opaque states. This can clearly be an annoyance, especially when the determination of a pixel being on is set by a simple threshold. It can be compensated for by having a calibrated threshold for each pixel in the detector plane. Should this not be desirable, or easy to implement, this can be compensated for by increasing the signal to noise. Should the transmission uniformity be only about ± 10 percent, this would require that the SNR be increased by about 20 percent, to compensate for this effect. To increase the SNR by 20 percent would require that the PPB now be increased to about 1500 photons/pixel.

Based on the above considerations it would seem that the primary requirement upon the SLM is uniformity and not contrast (although they are probably related). For the demonstration, a liquid crystal display would probably be adequate, while a high performance SLM would be desired for the large scale system because of its compact nature and greater speed.

6 Experimental Plan for Phase II

This section discusses the results of Task 4 of our Phase I Statement of Work, Development of an Experimental Plan to Investigate 4D Interconnects. In this section, we will describe in detail our plan for an experimental demonstration of our 4D interconnect concept.

The major issue to be addressed during our Phase II work is the experimental confirmation of the analysis and simulation performed by SPARTA prior to and during our Phase I contract. The experimental plan to read and write holographic gratings is described in Section 6.** Our experimental configuration has been defined in such a way that implementation of a feedback loop will be easily achieved, and this configuration will be described in Section 6.**.

The demonstration, described in Section 6.**, will be a low-end realization of an entire optical neural network architecture. This plan will examine the possible applications, the competition to optics in each of these areas, and the requirements in terms of cost, size, weight, and performance. Based on this investigation, a sample problem will be chosen as the basis for a demonstration.

6.1 Materials Selection for 4D Neural Net Experiments

A survey of the literature concerning candidate SHB materials has been made. A bibliography of the references consulted during this survey is presented in Appendix A. It is concluded that the optimal choice (at this time) for a host material would be polyethylene. The preferred photochemical species have been reduced to a group of four prime candidates. It is believed that the selection of one or two of these species for experimental use in Phase II of our program should provide a suitable vehicle to demonstrate the short term and long term capabilities of a 4D neural net based on these materials.

From our Phase I work, it is clear that many of the SHB materials which have been widely studied by previous workers are prime candidates for consideration in holographic storage applications. Therefore the materials selection task is not a significantly difficult one, but it does require some thought and care so as to provide results which can properly represent the true capabilities of these materials when addressing the 4D neural net application.

The primary requirements for a high end application device permitting 10^{12} interconnects within a 1 cm^3 volume are represented in Figure 32. This diagram bounds the parametric space related to photochemical quantum efficiency and absorption cross section. A secondary requirement is that the homogeneous linewidth should be less than or equal to 90 MHz. This homogeneous linewidth requirement has some assumptions behind it concerning the inhomogeneous linewidth. In particular, it was assumed that the useful inhomogeneous linewidth was approximately 9 THz wide. It is known that the selection of the host and of the photochemical species can both influence the inhomogeneous as well as the homogeneous line widths. Furthermore, it is easy to envision using several photochemical species in the same host material to effectively enhance the frequency range of operation. This approach seems quite feasible because several of the favorite host materials (such as polyethylene (PE) and polymethylmethacrylate (PMMA)) have been used by a number of researchers for a reasonably wide range of photochemical species.

With respect to the requirements of the early experimental demonstration of the 4D neural net having a modest capacity, almost any reasonable SHB material would probably be adequate. However, since the most commonly studied materials are also the ones which are expected to provide high performance for the high end application system, it would seem reasonable to restrict ourselves to the same set of materials so as to gain valuable practical experience with them in terms of direct 4D neural net applications.

6.1.1 Selection of Host Material

There are six principal requirements for the host material:

1. The photochemical species must be soluble in the host to a level which is determined by the absorption cross section. For the proposed 4D neural net, the material thickness required is of the order of 0.5 cm, and the optical density required is 1 for absorption holograms and 100 for phase holograms. The boundary on doping density corresponding to 1 percent also represents the boundary of spectral diffusion. Therefore, all of the photochemical species shown in Figure 32 have only modest solubility requirements of the order of 0.01 percent or less for absorption hologram applications. For phase holograms (where higher molecular densities are desired) in organic species (H_2P and H_2Pc) the solubility requirements are again not severe, but the inorganic species (F_4^-

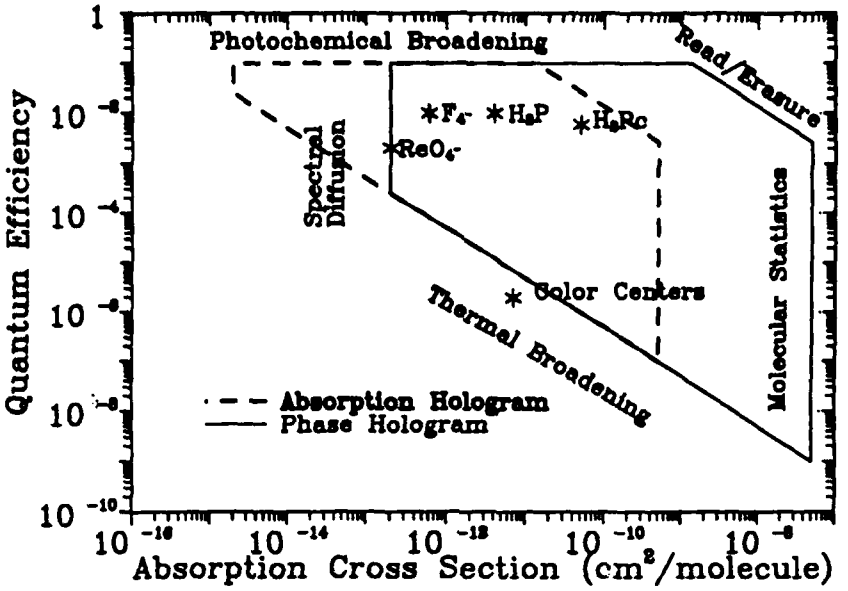

Figure 32. Allowed region of quantum efficiency and absorption cross section for a high end holographic 4D neural net application.

and ReO_4^-) may be reaching solubility limitations. Because organic species generally require organic hosts, we shall focus our attention on organic hosts.

2. The host must be optically clear. This is mostly a matter of material preparation, and previous workers have described simple techniques which have been used to achieve the quality necessary.
3. The host must be either a glass (random structure) or a partially crystalline structure. This provides a widely varying molecular environment around each photochemical species.
4. The host must be capable of absorbing and conducting away significant amounts of heat while at very low temperatures. The selection of a host should not be completely governed by this requirement, but if high data rates are desired and thermal broadening is to be avoided, as well as having a high read to erasure ratio, then a more thermally conductive host may be desirable. This desire, however, may be in conflict with the basic need for a glassy material, as thermal conductivity is much better in crystalline materials.
5. The host should be relatively easy to handle and cast into samples of the order of 0.5 cm thick. This is a practical requirement, not a fundamental one, but it can be a significant one for the early experiments if the host is not well chosen.
6. The host should be chemically inert with respect to the photochemical species and it should also have fundamental properties which allow for long storage life of the spectral holes.

These requirements are generally well met by the common organic polymers polyethylene and polymethylmethacrylate. In fact these two hosts have been used in a substantial fraction of all the SHB research studies and have been used with most of the favored photochemical

species. The reasons for the favored use of these two host materials relates strongly to their ease of handling and preparation. Both thin film[35] and thick cast samples[36,37] can be readily prepared containing a wide range of organic photochemical species. The use of these host materials by a number of researchers points to the reasonably high solubility of the photochemical species in these materials. Their optical properties are excellent, providing samples of suitable optical clarity and uniformity when appropriate care is taken. The microstructure is effectively random for PMMA and can be partially crystalline or quite "glass like" for PE (depending on the manner of preparation). The thermal properties of these materials are typical of materials having a randomized structure, so they are quite representative. The preparation of these materials is quite simple, with little or no chemical synthesis required because they are readily available as "off-the-shelf" items in high purity and at modest cost. Being commonly used base materials in electronics and for household items, they are of course quite stable chemically. They have also been shown to provide spectral holes which have a measured long term persistence.[36]

Based on these attributes, we can readily narrow the field to these two host materials as the primary media into which to introduce the selected photochemical species.

6.1.2 Selection of Photochemical Species

It is of course assumed that the photochemical species selected must have the cross sections and quantum efficiencies which fall within the parametric region defined in Figure 32. The only significant requirements to permit experimental investigations of the selected species are largely practical ones related to spectral hole width, solubility in the host materials, and potential hazardous effects of the photochemical species selected. Luckily, much of the information related to hole widths and solubilities are already determined adequately and the toxicology of these material is not significant. Once introduced into the host matrix and solidified these photochemical species become chemically inert so as to make handling of no significant concern.

Within the constraint of being contained in the two selected host media, a number of interesting candidate photochemical species can be selected and have already been characterized adequately to prove useful in our planned experiments on 4D neural nets. The candidate materials are shown in Table VI [37,38,39,40]. This list of candidate materials shows that PMMA would appear to have a significantly wider homogeneous linewidth than PE for all the photochemical species listed. Despite the fact that the homogeneous width can be reduced further by lowering the temperature, PMMA seems to be quite inferior as a host material if a very high end (high storage capacity) application is desired.

For PE the homogeneous linewidth is within an acceptable range of the desired width of 90 MHz. Reducing the temperature can be an acceptable means to achieve the spectral hole width desired. The only tradeoff required is one concerning the conductivity and heat capacity of the material, which can impact operating speed and the read/erasure resistance of the stored information. Of the four photochemical species, all are subject to reversible photochemical changes except for DMST. This material decomposes when photochemically excited. For certain system applications this may prove to be an advantage, as it makes the storage operation quite permanent.

An interesting concept to explore experimentally is to have multiple photochemical species present in the same host. This concept would allow one to extend the effective frequency range for storage of information. Such a combination might be H_2P and resorufin in PE. The

Table VI. Properties of Selected SHB Materials

Material	Host	Temp.	Center Wavelength	Inhomogeneous Linewidth	Spectral Hole Width
H_2P	PE	4.2K	611 nm	4.5 THz	40 MHz
	PMMA	4.2K		4.5 THz	1.0 GHz
DMST	PE	4.2K	588 nm	9 THz	170 MHz
	PMMA	4.2K		9 THz	3.0 GHz
Resorufin	PE	4.2K	591 nm	30 THz	230 MHz
	PMMA	4.2K		30 THz	1.2 GHz
H_2Pc	PE	4.2K	693 nm	3 THz	500 MHz
	PMMA	4.2K		10 THz	10 GHz

DMST dimethyl-s-tetrazine
H_2P free base porphyrin
H_2Pc phthalocyanine
PE polyethylene
PMMA polymethylmethacrylate

center wavelengths are close enough that they would be accessible when using the same laser dye. While the absorption peaks are not close enough to permit overlap, it may be expected that suitable materials may be available in the future if this concept of multiple photochemical species can be shown compatible with the needs of a high end system.

The issues associated with quantum efficiency can be addressed directly in the future by some selective "engineering" of the photochemical species. This has been shown to be feasible[41] with a capability to alter the quantum efficiency of selected molecular structure by changing chemical side groups. This approach leaves the main properties of the photochemical species intact (homogeneous and inhomogeneous width) while altering a major factor which can directly affect system performance. It can be expected that similar chemical modifications to the critical components of the SHB materials (host as well as photochemical species) will be carried out in the future in order to optimize performance.

The optimal selection of photochemical species can also be influenced by the availability of tuneable laser sources. A material such as H_2Pc becomes attractive when the laser source is considered because it comes within the range of a solid state Ti:Al_2O_3 laser. Furthermore, semiconductor diode lasers which are tuneable in the region below 700 nm are presently under development[42] and would make SHB materials which can be used in that wavelength range attractive for providing a compact overall system.

From the above analysis, it can be seen that PE would seem to be the superior host material. The four candidate photochemical species are all of significant interest in the planned experimental program as they have been well studied and have properties which can have long term applications interest. It is therefore planned to experimentally consider only polyethylene as the host material for our Phase II experiments, with one or two of the photochemical species listed above being subject to in-depth testing and analysis.

6.2 Optical System Design for 4D Neural Net Experiments

An optical system design is presented in this section which incorporates all the necessary attributes of the 4D neural net architecture. The details are presented to a level which would allow direct purchase and costing of the specific optical elements. The optical design satisfies all the requirements for the initial grating experiments as well as for a significant demonstration. The design presented would allow for direct interconnection of two 64 by 64 element planes, which translates into roughly 1.6×10^7 interconnects.

The fundamental architecture of the proposed 4D neural net system has been shown in Figure 33. The major components are the SHB material itself, two input plane SLMs and two output plane detector arrays. One of the SLMs is illuminated fully at each frequency, while the other has only one column illuminated by each frequency. The illumination is provided by a multi-frequency laser, which has the capability of providing either a singly selected frequency, or a complete comb of 64 frequencies simultaneously. Electronic feedback is provided by digital read-out of the CCD arrays, the data from which can then be directly used to control the individual pixels in the SLM. The primary attributes of "storage" and "feedback" can then be clearly demonstrated with this fundamental architecture.

To properly implement this architecture with efficiency in light usage and to provide high contrast holograms requires the careful implementation of some relatively standard optical principles and a detailed optical design. One also has the ancillary requirement that the components used for this first experimental demonstration of a 4D optical neural net be commercially available and be implemented with a minimum of complexity and cost. These compromises require that the experimental system proposed here be larger than a working system might be and actually have more components than the working system. With these compromises in mind, the general layout of the experimental optical system is presented in Figure 35. The primary segments of the system and will each be examined in sufficient detail to understand and implement each of the necessary functional properties.

The general layout of the system is in two parallel optical trains which are spaced 8 cm apart. These two trains are of approximately equal length and are located in close proximity to minimize the effects of air turbulence upon the stability of the laser beams. The total length is approximately 1 meter, and the total width and height is less than 12 cm, allowing the system to be covered to minimize turbulence and eliminate stray light, as well as to be designed into a brassboard configuration. All components will be antireflection coated (when possible) to reduce scatter and enhance system performance.

The complete system is divided into four sections which can be treated as largely independent of each other. This independence will not only aid in the following discussions but also in their implementation during the program. These sections are:

1. Cryostat and Detector Optics,
2. SLM and Reduction Optics,
3. Dispersion and Beam Expansion Optics,
4. Laser and Beam Shaping Optics.

The electronic feedback is not shown and will be discussed in Section 6.3.

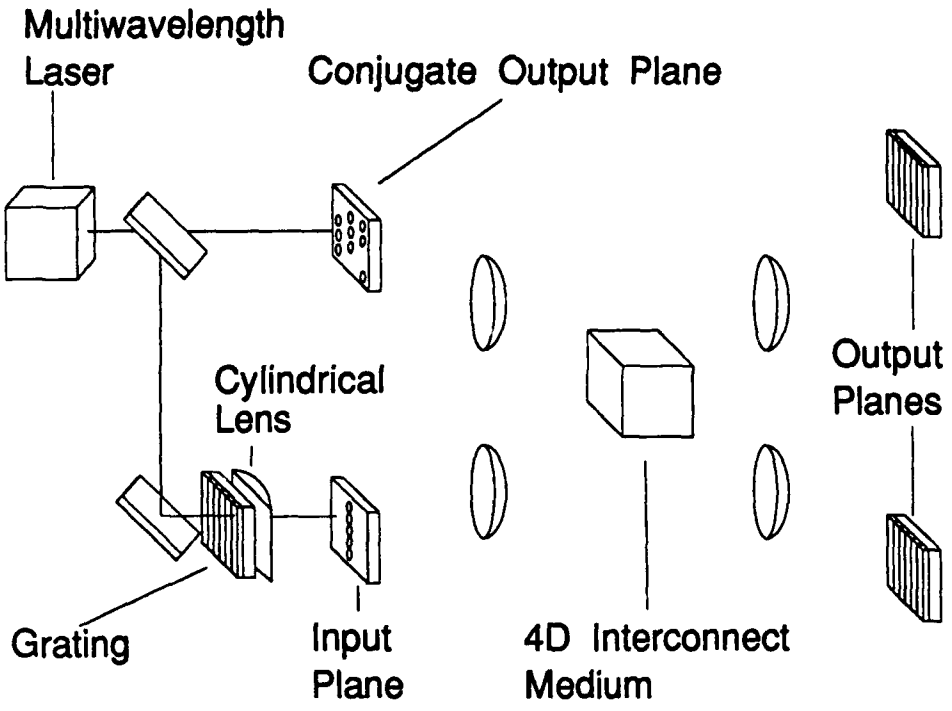

Figure 33. Schematic optical layout for the experimental version of the proposed 4D neural net computer.

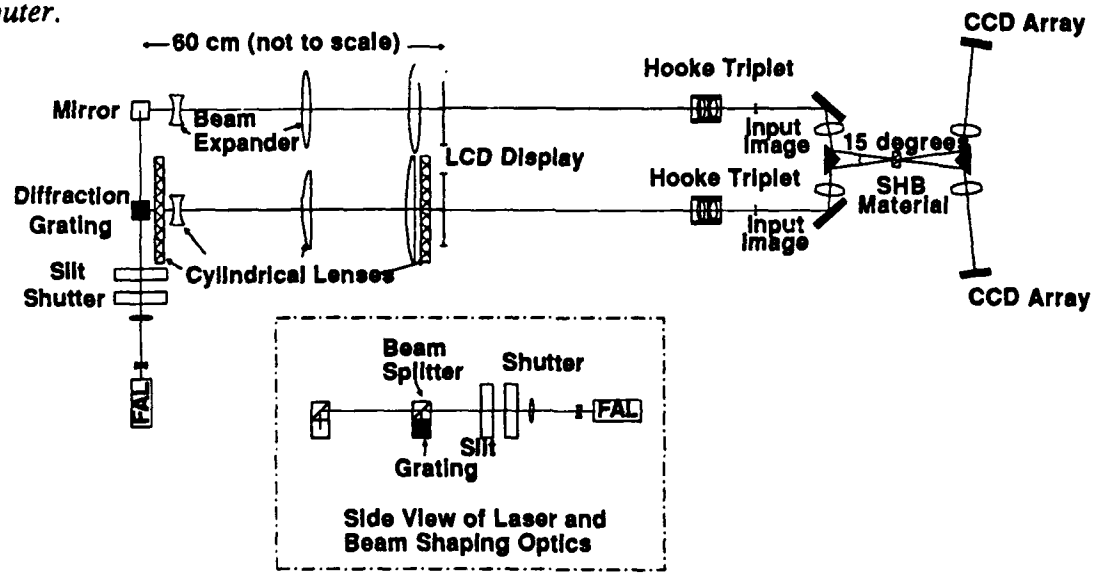

Figure 34. General layout of the proposed optical system for the experimental 4D neural net.

6.2.1 Cryostat and Detector Optics

This segment of the system contains the central input and output optics of the neural net and is shown in detail in Figure 35. It is largely symmetric with each of the four separate legs of the system having nearly identical optical properties. The two input images are brought to a focus at the left side of the figure and the pupils of these simple lenses are located inside the SHB material. The two beam paths have an angle of 15 degrees with respect to each other and are simply combined and later split by the reflective prisms. After passing through the SHB material, the beams are again separated, with each being reimaged onto the cooled CCD detector arrays.

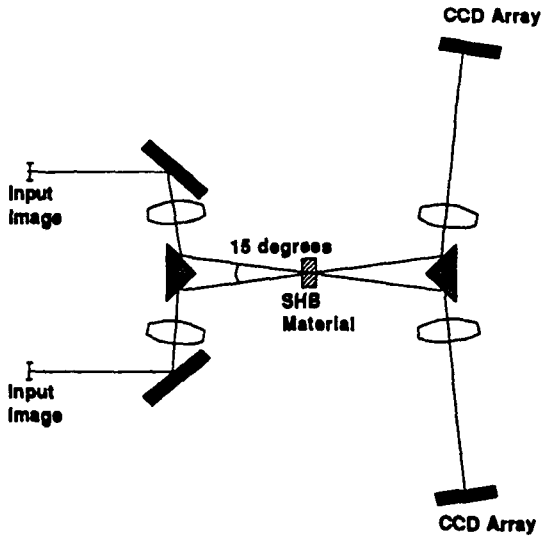

Figure 35. Details of the optical elements surrounding the SHB material (located in the cryostat) and the elements leading from the immediate input to the output planes.

Each of the four lenses has focal lengths of 6 cm and the laser mirrors shown are flat to $\lambda/10$ over 25 mm. The entrance pupil diameter is set by the area of the SHB material which will be used for storage, which is 0.5 cm diameter. This makes this section of the system have an F number of 12, which leads to a resolution of 8.4 μm at 700 nm. This well exceeds the image resolution required which is 0.5 cm/64 pixels, or 78 μm between pixels.

Component	Melles Griot Part Number	Number Required
Lens	06-LAI-007	4
Mirrors	02-MFG-001	2
Mirror-Coated Prism	01-PRS-013	2

The two CCD detector arrays selected will be 12 bit slow scan CCD arrays from Photometrics. This array is thermoelectrically cooled to -45 C, is programmable, and has frame storage capabilities. The frame time is electronically selectable.

6.2.2 SLM and Reduction Optics

The principal function of this segment of the system (see Figure 36) is to reduce the image size of the SLM. We have chosen to utilize LCD (liquid crystal displays) as the input planes for our experimental system due to cost and convenience considerations. The advantages of LCD displays are that they are readily available as personal computer displays of significant resolution and already have the necessary hardware and software available to present any image to the neural net in a convenient and adequate contrast format. Moreover, because of the size of the LCD displays, both input planes can be represented on the same LCD display, with the images automatically synchronized. These factors can significantly reduce the complexity of this component of the system, while potentially allowing quite sophisticated images to be presented to the system for storage and analysis.

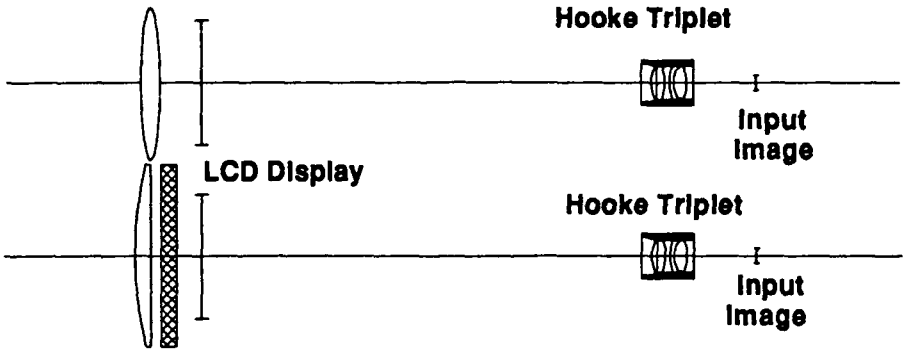

Figure 36. Details of the optical elements which permit reduction of the image provided by the LCD.

The penalty which must be paid for using the LCD displays (instead of a more sophisticated and compact SLM) is that the illuminating beams must be broadened to about 3.6 cm diameter and the images must be significantly reduced. We have chosen to provide an intermediate image of the LCD images before entering the cryostat and detector optics to permit inspection of the images for experimental purposes.

The reduction is carried out by use of a simple Cooke triplet having a focal length of 3 cm and an entrance pupil of 1.07 cm. The Cooke triplet is a high resolution component which will certainly not limit optical performance over a field of 1.06 cm (the required image field is only 0.7 cm). The use of a simple triplet to carry out the reduction requires that the illumination optics focus the light at the pupil of the triplet. The illumination optics will be discussed in the following section.

Component	Melles Griot Part Number	Number Required
Cooke Triplet	01-LAS-001	2

The selection of a personal computer is not necessarily critical since they all have comparable pixel resolution and generally acceptable screen size. The PC selected will be an IBM PC or compatible which will readily permit interfacing with the output plane CCD cameras and utilization of simple software compatible with other PC's at SPARTA to permit writing of software off-line. The use of a PC may even permit direct use of graphics packages for image construction. A specific requirement of the system is that the LCD screen have gray scale capability. Gray scale capability permits reliable convergence of the neural net under feedback. Gray scale is now available on some laptop PCs such as the Compaq SLT/286 which has 8 levels of grey at 640 × 480 resolution, or 16 levels at 320 × 200 resolution.

In actual use, the display must be partially disassembled to permit transmission of the laser beam through it. Optical flats can be optically coupled to the front and back surfaces of the LCD should it be determined that the wavefront distortion of the display must be improved upon. We may also choose to remove the glare prevention coverglasses to enhance transmission for some experiments.

6.2.3 Dispersion and Beam Expansion Optics

This segment of the optical system is optically simple, although conceptually complex. The complexity arises in one of the legs of the optical system from the need to carry out dispersion of the laser beam on one of the optical dimensions without expanding the beam in that dimension, while expanding the beam in the other dimension. The other leg of the optical system is a simple beam expansion and illuminator.

We shall describe the simple symmetric beam expansion which occurs on optical leg A (see Figure 37). After being reflected off the mirror (a), the laser beam is already a 3 mm square parallel beam which needs to be expanded by 10× to permit appropriate illumination of the required segment of the LCD display. To carry this out a simple pair of lenses (b and c) are used to expand the beam and retain its parallel path. The light remains parallel until just before the LCD display at which point it is focused by a simple lens (d). The focal point of lens (d) is the pupil of the Cooke triplet. The functions of lenses (c) and (d) could have been combined into a single element, but we chose to separate them in order to simplify the optical setup.

On optical leg B, the beam expansion which occurs is nearly identical to that seen in leg A except that the expansion desired occurs in only one dimension. This is simply carried out with cylindrical lenses. The dispersion of the beam with frequency is carried out by use of a simple holographic grating (e) having 2400 lines/mm. A 3 mm segment of the grating is illuminated by a parallel beam. Over a length of 60 cm, this would permit a 10 nm wide segment of the spectrum (at 700 nm) to be dispersed over 2.5 cm (the size of the 64 by 64 segment of the LCD array). The finesse of the grating will be more than adequate to permit individual illumination of a single column of pixels on the LCD display.

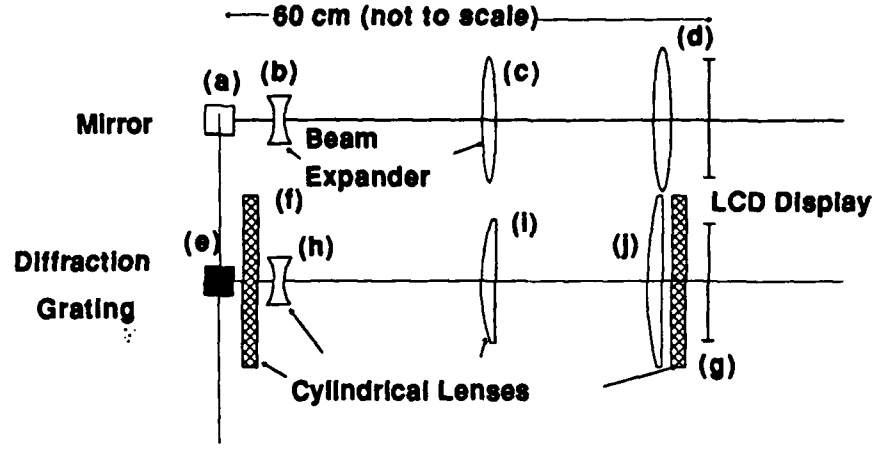

Figure 37. Details of the optical elements which expand the illuminating laser beams and also direct the beam as a function of laser wavelength.

To achieve the single column illumination one also needs to focus the beam using a simple cylindrical lens so that it is reduced from 3 mm down to the required 0.4 mm at the LCD array. The focusing is simply achieved with a lens having a focal length of 60 cm (f). The resolution of lens (f), illuminated by a 3 mm beam, will permit an illumination stripe 140 μm wide (more than adequate resolution). Just before reaching the LCD, the beam passes through another cylindrical lens (g) which causes the illuminated region of the LCD to be focused in the pupil of the Cooke triplet. Beam expansion in the other dimension is carried out similarly to the manner seen in leg A, by use of cylindrical components (h and i). Just before passing through the LCD, another cylindrical lens (j) focuses the beam in the pupil of the Cooke triplet.

Component	Melles Griot Part Number	Number Required
(a) Concave Lens	01-LDK-001	1
(b+c) Convex Lens	01-LDX-222	2
(d) Diffraction Grating	N43,224*	1
(f) 2 Cylindrical Lenses	01-LCP-015	1
	01-LCP-012	1
(g) Cylindrical Lens	01-LCP-013	1
(h) Cylindrical Lens	01-LCN-002	1
(i) Cylindrical Lens	01-LCN-013	1
(j) Cylindrical Lens	01-LCN-015	1

* Edmund Scientific.

6.2.4 Laser and Beam Shaping Optics

This section of the optical system merely has the function of providing a coherent source of light which is collimated, shaped, and split into two beams to enter the two separate legs of the optical system. As can be seen in Figure 38, these operations are accomplished by expanding the beam to a diameter of 5 mm and then passing it through a 3 mm square aperture. The collimated beam then passes through an electronic shutter and a 50 percent beam splitter which sends half of the light into leg B and the other half of the beam into leg A.

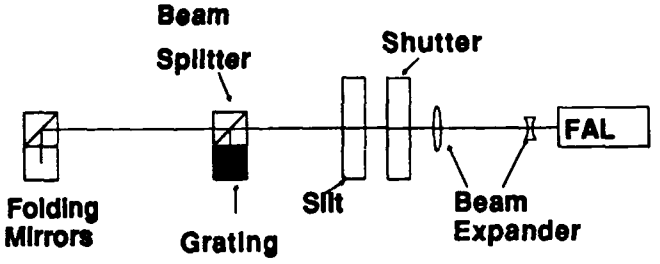

Figure 38. Details of the optical elements which expand and shape the illuminating laser beams. After shaping, the beam is then split to permit simultaneous illumination of the two legs of the system.

The requirements on the laser itself are much more significant. The minimal requirements are that the laser be tuneable over a range of 10 nm in the vicinity of 550 to 650 nm. For minimal experimental needs, rapid tuning and digital control are not required. For suitably rapid experimentation however, it will be worth having a frequency agile system which can be computer controlled with reasonably rapid tuning capability. In this wavelength region, a tuneable dye laser would be a convenient choice. The pump source would be an Argon-ion laser. Digital control would be provided by a PC which can be directly linked to the computer which controls the LCD as well as the CCD arrays and the electronic shutter.

A potential option would include the capability of the laser to provide a "comb" of laser frequencies at regularly spaced intervals matching the frequencies at which holograms are stored in the SHB material. Thus, a comb of laser frequencies would allow simultaneous illumination of all pixel columns on both input planes for full and symmetric interconnection of the 2 input planes. Producing such a comb of frequencies might be accomplished by mode locking the laser. This might require an electro-optic modulator with a frequency of operation in the range of 1 GHz to obtain the necessary laser frequency spacing for some applications. If such a comb of illumination frequencies is not available, the frequency agile laser (FAL) could be used to rapidly scan through the laser wavelengths of interest and the total resultant signal stored by the CCD arrays over the complete scan period. In either case, functionality required for the experiment can be achieved.

Because of the high sensitivity of the SHB materials of interest, the power requirements on the FAL would be minor (10 mW or less). To provide interesting storage capability and frequency selectivity, these experiments would be adequately carried out with frequency selectivity of the

order of 300 MHz, which is readily obtainable from the SPARTA FAL.

6.2.5 Incrementally Assembling the Complete Design

The initial experiments which will provide important information on material performance and optical details will not require much of the optics in the complete design shown above. To write simple gratings will only require the modest beam expansion and splitting seen in the Laser and Beam Shaping section, coupled with the few mirrors and the CCD cameras seen in the Cryostat and Detector optics section (see Figure 39). This configuration will permit storage of gratings at several independent frequencies. With a modest capability to alter the beam angle on leg B, the experiments which demonstrate storage of multiple interconnects at the same frequency can be carried out. By introducing computer controlled scanning of the FAL, one or more "frequency channels" can be bleached in the SHB material.

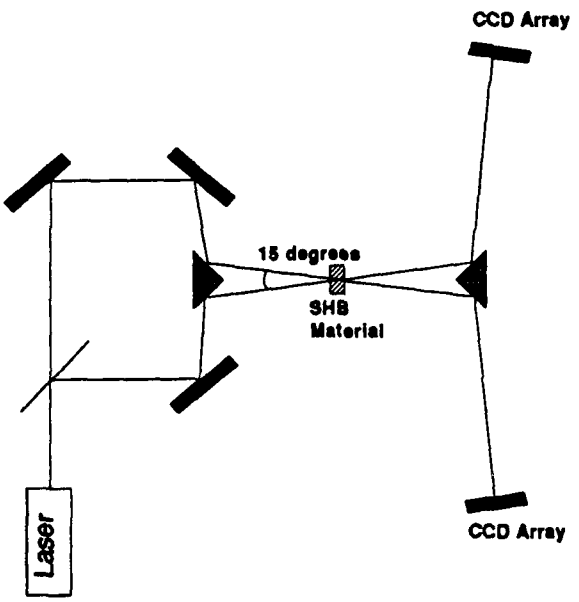

Figure 39. Details of the optical elements required for the initial recording of simple gratings. By incrementally expanding on this simple layout, the complete system can be built up.

Finally, the LCD display with feedback from the CCD arrays can be provided, which will result in an operational 4D neural net.

6.2.6 Summary of Experimental Design

An experimental optical design is presented which both meets the needs of the final complete 4D neural net system. This design can be built up in segments and introduced as the program proceeds though the necessary experiments. All the components are either commercially available, or can be readily obtained by minor mechanical modification of existing components. The approach of building up the system in pieces will permit section by section implementation and set-up of the system, with a minimum of cost and rework.

It is also worthy of note that the system outlined above is significantly "over-designed" at present, (even with off-the-shelf components) having greater resolution than really needed for these experiments. Without altering any other components, the pixel density of the SLM could be increased by a factor of 3 in each dimension. This expandability would effectively permit the total interconnect capacity of this system to reach 10^9. This clearly indicates the capability of the approach and the importance of the SLM in determining system performance.

6.3 Implement Device with Electronic Processing and Feedback Loop

The electronic feedback system required for the experimental 4D neural net is detailed in this section. It is entirely PC based using off-the-shelf components. Hardware development is not required and the software required for experimental diagnostics and data taking is minimal. Software required for full system operation is modest.

6.3.1 System Requirements

The two principal attributes necessary to neural net functioning are (1) information storage and (2) feedback. The information storage is carried out by the use of the SHB material as a holographic recording medium. The feedback can be accomplished either optically or electronically, however, the feedback must include gain. The application of gain is most easily achieved electronically in an experimental system as well as in a high end system. Since the nature of the 4D system allows direct pixel to pixel correspondence in a dense regularly arranged manner (not fractal) the feedback is quite simple and can be readily accomplished under personal computer (PC) control. The advantage of the electronic feedback approach is that the correspondence between output pixels and input pixels can be changed at will (through software) as can the gain. This flexibility permits the experimental neural net design to be considered a very general one.

Since this is an experimental system, necessary attributes of the system are that it be easy to work with, assembled from reliable components, permit data extraction directly at a number of key locations and at the several stages of experimental development. It is believed that the proposed system meets these requirements and should significantly assist in the planned experimental program in all stages of development.

6.3.2 System Description

A schematic overview of the system is seen in Figure 40. The key property of the system is that a cyclic flow of information occurs in the system in a manner which allows direct feedback to occur between the output CCD detectors and the input LCD display. It is argued that the use of electronic feedback in an optical neural net architecture is not simply a convenience allowed for experimentation but can be considered a realistic approach to a large scale system. Since the information content of the input and output planes is the square root of the information content of the neural net itself, the data transfer rate between input and output planes can be of the order of 1 MHz while the internal processing speed of the neural net would be equivalent to 1 THz. By this simple (and easily realistic) argument, it can be seen that the use of electronic feedback should not provide a performance limitation to the operational speed of the total system. The fact that feedback is accomplished electronically also allows us to take advantage of off-the-shelf hardware and software which is commercially available.

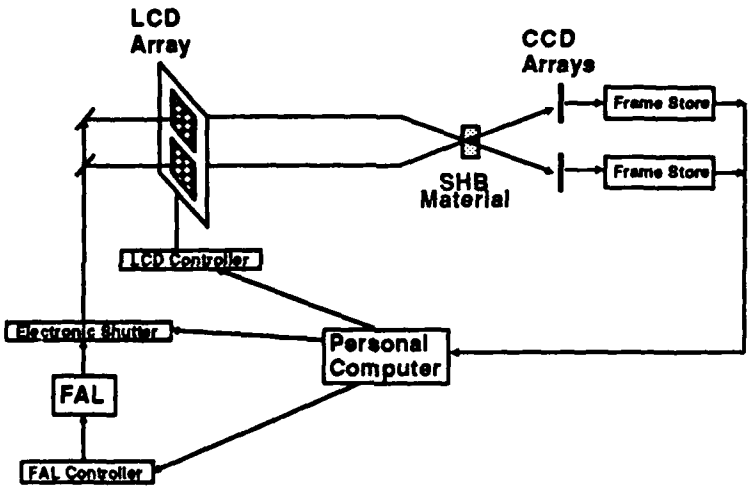

Figure 40. Schematic of the complete 4D neural net system highlighting aspects of the electronic feedback loop.

The major components of the experimental feedback system are:

1. CCD arrays with frame storage capabilities,
2. LCD display and controller,
3. FAL and controller,
4. Electronic Shutter,
5. Personal Computer.

6.3.2.1 CCD Arrays

The detector arrays will be commercially available CCD arrays which can be operated cooled, with slow scan, and with frame storage capabilities. The above attributes permit very low noise operation and efficient light collection. The frame storage capability allows the images to be studied in detail and readily examined or manipulated in order to diagnose optical system performance or be fed back to the LCD arrays. The frame storage units may be purchased as part of the camera control units or may be frame grabber cards inserted into the personal computer. Frame transfer back to the PC is accomplished digitally through an IEEE 488 interface card which is PC interface compatible.

6.3.2.2 LCD Display and Controller

The developments in the PC industry have made this particular component easy to obtain and use as it can be simply a laptop PC which has an LCD display. The LCD display must be partially disassembled to permit transmission of the laser beam. The laptop PC can be used as the controller itself with fully programmable capabilities including grey scale and reliable interface to the master PC or directly from the CCD camera frame storage units. Being a fully operational PC one can also make use of readily available graphics software to permit display of detailed images on the LCDs for input to the neural net.

6.3.2.3 FAL and Controller

This component of the system will be a dye-based frequency agile laser (FAL) pumped by an Argon-ion laser. The FAL system is manufactured by SPARTA and will be available for use during the later stages of the program. The FAL is controlled by a PC system of its own, with easy interface capabilities to the master PC system.

6.3.2.4 Electronic Shutter

This component will simply be an electronic shutter which can be directly controlled by the master PC.

6.3.2.5 Personal Computer

This component is the central control point for system control and feedback of information from the CCD arrays. While the controllers from the FAL or the LCD systems could have provided the capability demanded by the overall system to meet the functions of central control and data manipulation, such operation would have been clumsy at best, for experimental purposes. Therefore, having a PC dedicated to being the central control unit of the system will permit complete experimental flexibility with maximum data acquisition analysis and control being possible in a minimum amount of time. Being fitted with IEEE 488 and other standard interface cards, this unit will be able to communicate directly with all major system components in a timely manner.

6.3.3 Summary of the Feedback System

It is readily seen that the electronic feedback system can be directly implemented with a minimum of effort and with little software development. From the earliest stages of introduction, the system can be extremely helpful in the experiments to provide easy and detailed examination of the results. The electronic system proposed will not only permit full electronic feedback capability but will enhance the efficiency of the entire experimental effort allowing us to concentrate our efforts on the more fundamental issues surrounding the recording of holograms in SHB materials.

6.4 Demonstration System

Construction of a demonstration system is a critical milestone in the progression toward future application of this work. The key is to choose a system which is both within reach during a Phase II effort and has significant capability.

Our demonstration system will be the culmination of all our Phase II experimental work. We will begin by first recording a single interconnect grating and then multiple interconnect gratings. We will add spatial light modulators at the input and detector arrays at the output during the second part of the experimental program. To complete the demonstration system we will incorporate a microcomputer to implement the feedback loops and provide the non-linearities required for general purpose network operation.

Our goal for our Phase II demonstration is a system with the potential for up to 10^7 interconnects and 10^7 to 10^9 interconnects per second. A system meeting these specifications would exceed the capability of any electronic neural network implementation. This system can be achieved using an input SLM with a frame size of 64 by 64 and a frame rate of 1 to 100 Hz. Binary SLMs can achieve these characteristics by using larger frame sizes and combining binary pixels to achieve gray level performance using spatial dithering.[43] At these network performance levels the computational power of a microcomputer is sufficient to implement the non-linearity and feedback loops.

Choosing an appropriate problem will be a key to a successful demonstration. For example, we need a problem which is simple enough that "it can be solved in less than 10 years." This suggests a "toy problem" which is a reduced version of some real world problem. We also want to show off the capabilities of this approach, however.

Within the scope of a Phase II SBIR, it may not be possible to train the network to solve a problem which actually requires 10^7 interconnects and 10^7 interconnects per second. We may instead choose a toy problem which is clearly extendable to a real problem, and implement on hardware which is clearly capable of handling the larger number of interconnects and higher interconnect rate. Government personnel have offered to provide input to our choice of demonstration problem.[44]

7 Summary

All the key elements of the Phase I statement of work have been examined and reported on in depth. The results of these examinations point a clear direction for achieving success in the proposed Phase II effort, as well as indicate the immense long term potential of the approach for the ability to fabricate large capacity neural nets using SHB materials.

The analytical models of SHB materials developed point to a new approach of hologram storage in materials which are f ındamentally absorptive. The novel frequency channel approach has the potential for providing efficient storage of phase holograms which can minimize absorptive losses while increasing hologram efficiency, thereby permitting an extra degree off freedom in system design. This extra degree of freedom might be used to enhance capacity, operating speed, erasure resistance or other system properties of importance for specific applications.

The proposed architecture of the 4-D neural net system has been shown to be quite general by direct analysis of the requirements behind several important networking approaches. All of the major requirements of a neural net (including learning) can be met by the architecture selected, and based on SHB materials. It has been found that electronic feedback loops (properly implemented) should provide excellent performance to be met by the 4-D system, in an efficient and compact format. An analysis has been performed which directly relates the performance of a high end system to the fundamental properties of the SHB materials. This analysis shows that the presently investigated materials are well suited to the proposed architecture, arguing that materials development is not required before achieving success in a demonstration system.

SLM requirements were examined relating to the architecture analysis performed above with the result that presently available SLM's permit a demonstration of the 4-D system concept to be readily performed. Furthermore, the specifications of the SLM's presently under development will provide the capacity and performance necessary for implementation of the potential high end system.

Finally, the above analyses have permitted us to design a set of critical experiments which will examine the critical material properties and permit rapid implementation of the 4-D architecture. These experiments will culminate in the development of a demonstration system which will be capable of exhibiting the fundamental characteristics of the 4-D neural net architecture.

In conclusion, our analysis has shown that high capacity neural net systems based upon the natural 4-D properties of SHB materials are possible. Moreover, demonstration of these fundamental capabilities can be directly achieved in an experimental program using readily available components and materials.

References

1. DARPA Neural Network Study, Final Report, MIT/Lincoln Laboratory (18 July 1988).
2. APD Cryogenics, Inc., 1919 Vultee St., Allentown, PA 18103.
3. DARPA Neural Network Study, Final Report, MIT/Lincoln Laboratory (18 July 1988).
4. J. Gleick, *Chaos: Making a New Science,* (Penguin Books, New York) 1987.
5. D. Psaltis and N. Farhat, "Optical information processing based on an associative-memory model of neutral nets with thresholding and feedback," Opt. Lett. **10** (1985) 98.
6. K. Hsu, H-Y Li, and D. Psaltis, "Optical implementation and analysis of a two-layer heteroassociative memory," OSA Annual Meeting (Orlando, FL) 1989.
7. D. Psaltis, X. Gu, and D. Brady, "Fractal sampling grids for holographic interconnections," SPIE Proceedings **963** (1988) 468.
8. W. E. Moerner, ed., *Persistent Spectral Hole Burning:< Science and Applications,* (Springer-Verlag, New York) 1988.
9. D. E. Rumelhart, G. E. Hinton, and R. J. Williams, "Learning internal representations by error propagation," in *Parallel Distributed Processing: Exploration in the Microstructure of Cognition, Vol 1: Foundations,* D. E. Rumelhart and J. L. McLelland, eds., (MIT Press, Cambridge, MA) 1986.
10. R. M. Macfarlane and R. M. Shelby, "Homogeneous line broadening of optical transitions of ions and molecules in glasses," J. of Luminescence **36** (1987) 179.
11. H. P. H. Thijssen and S. Volker, "Spectral hole burning in semicrystalline polymers between 0.3 and 4.2K," J. Chem. Phys. **85** (1986) 785.
12. W. Lenth, R. M. Macfarlane, W. E. Moerner, F. M. Schellenberg, R. M. Shelby, and G. C. Bjorklund, "High-density frequency-domain optical recording," Proc. SPIE **695**, Optical Mass Data Storage II, (1986) 216.
13. A. R. Gutierriz, J. Friedrich, D. Haares, and H. Wolfrum, "Multiple Photochemical Hole Burning in Organic Glasses and Polymers: Spectroscopy and Storage Aspects," IBM J. Res. Dev. **26** (1982) 198.
14. M. Romagnoli, W. E. Moerner, E. M. Schellenberg, M. D. Levensen, and G. C. Bjorklund, "Beyond the bottleneck: submicrosecond hole burning in phthalocyanine," J. Opt. Soc. Am. **B1** (1984) 341.
15. A. Renn, A. J. Meixner, U. P. Wild and F. A. Burkhalter, "Holographic Detection of Photochemical Holes," Chem. Phys. **93** (1985) 157.
16. U. Itoh and T. Tani, "Research activities on materials for wavelength-multiplexed optical recording in Japan," Appl. Opt. **27** (1988) 739.
17. U. P. Wild, S. E. Bucher, and F. A. Burkhalter, "Hole burning, Stark effect, and data storage," Appl. Opt. **24** (1985) 1526.
18. W. E. Moerner and M. D. Levenson, "Can single-photon processed provide useful materials for frequency-domain optical storage?" J. Opt. Soc. Am. **B2** (1985) 915.
19. H. Kogelnik, "Coupled Wave Theory for Thick Hologram Gratings," Bell Syst. Tech. J., **47** (1969) 2909.
20. A. Yariv, *Introduction to Optical Electronics,* (1971, Holt, Rinehart and Winston, Inc.) 185.

21. J. J. Hopfield and D. Tank, "Collective Computation with Continuous Variables," to appear in: *Disordered Systems and Biological Organization,* (Springer-Verlag, 1986).

22. M. Minsky and S. Papert, *Perceptrons: An Introduction to Computational Geometry,* (MIT Press, Cambridge, MA) 1969.

23. G. E. Hinton and T. J. Sejnowski, "Learning and Relearning in Boltzmann Machines," in D. E. Rumelhart and J. L. McClelland, (Eds.) *Parallel Distributed Processing: Explorations in the Microstructure of Cognition,* (MIT Press, Cambridge, MA) 1986.

24. T. J. Sejnowski and C. R. Rosenberg, "NETtalk: A Parallel Network than Learns to Read Aloud," Johns Hopkins Univ. Tech. Report JHU/EECS-86/01.

25. R. P. Lippman, "An Introduction to Computing with Neural Nets," IEEE ASSP Magazine (April, 1987) 4.

26. D. E. Rumelhart, G. E. Hinton, and R. J. Williams, "Learning internal representations by error propagation," in: *Parallel Distributed Processing: Explorations in the Microstructure of Cognition, Vol. 1: Foundations,* D. E. Rumelhart and J. L. McClelland, eds. (MIT Press, Cambridge, MA) 1986.

27. K. Wagner and D. Psaltis, "Multilayer optical learning networks," Appl. Opt. **26** (1987) 5061.

28. J. P. Huignard, J. P. Herriau, and F. Micheron, "Selective erasure and processing in volume holograms superimposed in photosensitive ferroelectrics," Ferroelectrics **11** (1976) 393.

29. S. A. Burt, "High Speed Cameras for Machine Vision Applications," Electronic Imaging '89 West (April, 1989) 407.

30. R. W. Keyes and J. A. Armstrong, "Thermal Limitations in Optical Logic," Appl. Opt. **8** (1969) 2549.

31. C. Warde, A. D. Fisher, D. M. Cocco, and M. Y. Burmawi, "Microchannel spatial light modulator," Opt. Lett. **3** (1978) 196.

32. A. Rose and P. K. Weimer, "Physical Limits to the Performance of Imaging Systems," Physics Today **42** (September, 1989) 24 and the references noted therein.

33. R. C. Weast, Handbook of Chemistry and Physics, 50th edition, The Chemical Rubber Company, (1969), page D-129.

34. S. Burgess and D. Greig, Proceedings of the Fourteenth International Conference on Thermal Conductivity, Storrs CT, June 2-4, 1975, *Thermal Conductivity* **14**, Ed. by P. G. Klemens and T. K. Chu, Plenum Press, (1976) 45.

35. H. P. Thijssen and S. Volker, Chemical Physics Letters **120** (1985) 496.

36. T. Nishi, K. Arishima, H.Tabei and H. Hiratuka, Japanese Journal of Applied Physics **27** (1988) 225.

37. H. P. Thijssen and S. Volker, J. Chem. Phys. **85** (1986) 785.

38. H. P. Thijssen, R. Van Den Berg and S. Volker, Chemical Physics Letters, **120** (1985) 503.

39. A. R. Gutierrez, J. Friedrich, D. Haarer and H. Wolfrum, IBM J. Res. Develop. **26** (1982) 198.

40. W. E. Moerner, W. Lenth and G. C. Bjorklund, *Persistent Spectral Hole Burning: Topics in Current Physics,* ed. by W. E. Moerner, **44** (1988) 266.

41. N. Kishii, S. Tamura, N. Asai, K. Kawasumi and J. Seto, presented at SPIE LA 1989, Optical Data Storage Symposium, paper PDP-1.
42. J. Motodate, "Visible Laser Diodes: Opening the Way to New Applications," Photonics Spectra (December, 1989) 113.
43. M. Handschy, Display Tech, private communication, 12 April 1990; J. Waas, Semetex Corp., private communication, 12 April 1990.
44. B. Yoon, private communication, 4 April 1990.

APPENDIX A Appendix A

A Bibliography of Papers on Optical Neural Networks

Abu-Mostafa, Y. S., and D. Psaltis, "Optical Neutral Computers," Scientific American **256** (1987) 88.

Athale, R. A., H. H. Szu, and C. B. Friedlander, "Optical implementation of associative memory with controlled nonlinearity in the correlation domain," Optics Letters **11** (1986) 482.

Anderson, D. Z., "Coherent optical eigenstate memory," Optics Letters **11** (1986) 56.

Anderson, D. Z., "Optical systems that imitate human memory," Computers in Physics, (1989) 19.

Bian, S., K. Xu, and J. Hong, "Optical associative memory model with threshold modification using complimentary vector," SPIE Proceedings **963** (1988) 560.

Barnard, E., and D. Casasent, "New Optical Neural System Architectures and Applications," SPIE Proceedings **963** (1988) 537.

Barnard, E., and D. Casasent, "Optical neural net for classifying imaging spectrometer data," Appl. Opt. **28** (1989) 3129.

Brenner, K., and F. Sauer, "Diffractive-reflective optical interconnects," Appl. Opt. **27** (1988) 4251.

Batacan, P., "Can physics make optics compute?" Computers in Physics, (1988) 9.

Bell, T. E., "Optical crossbar switch to be developed for strategic computers," The Institute, (1985) 8.

Caulfield, H. J., "Variable and fixed rank N^4 interconnections," SPIE Proceedings **963** (1988) 564.

Changsuk, O., and P. Hankyu, "Real-time Fourier transformed holographic associative memory with photorefractive material," SPIE Proceedings **963** (1988) 554.

Chevallier, R. C., G. Y. Sirat, K. J. Haggerty, A. D. Marauni, "Frequency Multiplexed Raster Scheme of an Optical Neural Network: Shift Invariant Recognition," SPIE Proceedings **963** (1988) 522.

DeCusatis, C., P. Das, and D. M. Litynski, "Integrated optical implementation of the Hopfield neural network model," SPIE Proceedings **963** (1988) 497.

Feldman, M. R., S. C. Esener, C. C. Guest, and S. H. Lee, "Comparison between optical and electrical interconnects based on power and speed considerations," Appl. Opt. **27** (1988) 1742.

Feldman, M. R., and C. C. Guest, "Interconnect density capabilities of computer generated holograms for optical interconnection of very large scale integrated circuits," Appl. Opt. **28** (1989) 3134.

Fisher, A. D., and C. L. Giles, "Optical adaptive associative computer architectures," IEEE (1985) 342.

Fisher, A. D., W. L. Lippencott, and J. N. Lee, "Optical implementations of associative networks with versatile adaptive learning capabilities," Appl. Opt. **26** (1987) 5039.

Gallagher, R. T., "Holograph switches optical signals," Electronics (1985) 19.

Giglmayr, J., "Classification scheme for 3-D shuffle interconnection patterns," Appl. Opt. **28** (1989) 3120.

Glaser, I., and L. Perelmutter, "Optical interconnections for digital processing: a noncoherent method," Optics Letters **11** (1986) 53.

Goodman, J. W., "Optical interconnections in microelectronics," SPIE Proceedings **456** (1984) 1.

Guest, C. C., and R. TeKolste, "Designs and devices for optical bidirectional associative memories," Appl. Opt. **26** (1987) 5055.

Higgins, T., "A Breakthrough for Optical Neural Nets," Lasers and Optronics.

Ishikawa, M., "Experimental studies on adaptive optical associative memory," SPIE Proceedings **963** (1988) 527.

Kranzdorf, M., K. M. Johnson, L. Cotter, L. Zhang, and B. J. Bigner, "A Polarization Based Optical Connectionist Machine," SPIE Proceedings **963** (1988) 512.

Kyuma, K., J. Ohta, K. Kojima, and T. Nakayama, "Optical Neural Networks: System and Device Technologies," SPIE proceedings **963** (1988) 475.

Kinser, J. M., H. J. Caulfield, and J. Shamir, "Design for a massive all-optical bidirectional associative memory: the big BAM," Appl. Opt. **27** (1988) 3442.

Lee S., J. Jang, J. Park, and S. Shin, "Modification of the Hopfield model and its optical implementaion for correlated images," SPIE Proceedings **963** (1988) 504.

Lohman, G. E., and A. W. Lohmann, "Optical interconnection network utilizing diffraction gratings," Optical Engineering **27** (1988) 893.

Marom, E., B. H. Soffer, U. Efron, and Y. Owechko, "Associative memory neural networks with concatenated vectors," SPIE Proceedings **963** (1988) 546.

Marrakchi, A., "Continuous coherent erasure of dynamic holographic interconnects in photorefractive crystals," Optics Letters **14** (1989) 326.

McManus, J. B., R. S. Putnam, and H. J. Caulfield, "Switched holograms for reconfigurable optical interconnection: demonstration of a prototype device," Appl. Opt. **27** (1988) 4244.

Paek, E.G., J.R. Wullert II, and J.S. Patel, Bellcore, "Optical learning machine for multi-category classification," Optics News (1989) 28.

Peterson, C., and S. Redfield, "Adaptive Learning with Hidden Units Using a Single Photorefractive Crystal," SPIE proceedings **963** (1988) 485.

Psaltis, D., D. Brady, and K. Wagner, "Adaptive optical networks using photorefractive crystals," Appl. Opt. **27** (1988) 1752.

Psaltis, D., X. Gu, and D. Brady, "Fractal sampling grids for holographic interconnections," SPIE Proceedings **963** (1988) 468.

Psaltis, D., and N. Farhat, "Optical information processing based on an associative-memory model of neutral nets with thresholding and feedback," Optics Letters **10** (1985) 98.

Singh, J., S. Hong, P. K. Bhattacharya, and R. Sahai, "Quantum confined Stark effect of excitonic transitions in GaAs/AlGaAs MQW structures for implementation of neural networks: basic device requirements," Appl. Opt. **27** (1988) 4554.

Sirat, G. Y., A. D. Marauni, and R. C. Chevallier, "Frequency multiplexed raster neural networks. 1: Theory," Appl. Opt. **28** (1989) 1429.

Song, Q. W., and F. T. S. Yu, "Generalized perfect shuffle using optical spatial filtering,"

Appl. Opt. **27** (1988) 1222.

Soffer, B. H., and G. J. Dunning, Y. Owechko, and E. Marom, "Associative holographic memory with feedback using phase-conjugate mirrors," Optics Letters **11** (1986) 118.

Taboury, J., J. M. Wang, P. Chavel, and F. Devoes, "Optical cellular processor architecture. 2: Illustration and system considerations," Appl. Opt. **28** (1989) 3138.

Till, J., "Optoelectronic Scheme Opens Doors for Neural Nets," Electronic Design (1989) 27.

van der Lugt, A. V., "Design relationships for holographic memories," Appl. Opt. **12** (1973) 1675.

Weiss, S., M. Segev, S. Sterklar, and B. Fischer, "Photorefractive dynamic optical interconnects," Appl. Opt. **27** (1988) 3422.

Wherrett, B. S., "The many facets of optical computing," Computers in Physics, (1988) 24.

White, H. J., "Experimental results from an optical implementation of a simple neural network," SPIE *Proceedings* **963** (1988) 570.

White, H. J., N. B. Aldridge, and I. Lindsay, "Digital and analogue holographic associative memories," Optical Engineering **27** (1988) 30.

White, H. J., and W. A. Wright, "Holographic implementaion of a Hopfield model with discrete weightings," Appl. Opt. **27** (1988) 331.

Winthrop, J. T., and C. R. Worthington, "Theory of Fresnel Images. I. Plane Periodic Objects in Monochromatic Light," Journal of the Optical Society of America **55** (1965) 373.

Yariv, A., and S. Kwong, "Associative memories based on message-bearing optical modes in phase-conjugate resonators," Optics Letters **11** (1986) 186.

APPENDIX B Appendix B

A Bibliography of Papers on Spectral Hole Burning Materials

Burland, D. M., F. Carmona, G. Castro, D. Haarer, and R. M. Macfarlane, "Write and read scheme for photochemical hole burning storage systems," IBM Tech. Disc. Bull. **21** (1979) 3770.

Cadogen, K. D., and A. C. Albrecht, "Detailed Studies of a One-Electron, Two-Photon Ionization in a Rigid Organic Solution at 77 K," J. Phys. Chem **72** (1968) 929.

Chraplyvy, A. R., W. E. Moerner, A. J. Sievers, and R. H. Silsbee, "Persistent Nonphotochemical Hole-Burning of a Molecular Vibrational Mode in Alkali Halide Lattices," Appl. Phys. B **28** (1982) 264.

de Vries, H., and D. A. Wiersma, "Homogeneous Broadening of Optical Transitions in Organic Mixed Crystals," Phys. Rev. Lett. **36** (1976) 91.

Friedrich, J., and D. Haarer, "Photochemical Hole Burning: A Spectroscopic Study of Relaxation Processes in Polymers and Glasses," Angew. Chem. Int. Ed. Engl. **23** (1984) 113.

Friedrich, J., and D. Haarer, "Tunneling and Relaxation Processes in Organic Glasses as Studied by Photochemical Hole Burning," Appl. Phys. B **28** (1982) 262.

Friedrich, J., D. Haarer, and R. Silbey, "Reversible and Irreversible Line Broadening of Photochemical Holes in Amorphous Solids," Chem. Phys. Lett. **95** (1983) 119.

Gutierrez, A. R., J. Friedrich, D. Haarer, and H. Wolfrum, "Multiple Photochemical Hole Burning in Organic Glasses and Polymers: Spectroscopy and Storage Aspects," IBM J. Res.

Develop. **26** (1982) 198.

Huston, A. L., and W. E. Moerner, "Detection of persistent spectral holes using ultrasonic modulation," J. Opt. Soc. Am. B **1** (1984) 349.

Itoh, U., and T. Tani, "Research activities on materials for wavelength-multiplexed optical recording in Japan," Appl. Opt. **27** (1988) 739.

Janowiak, R., and H. Bassler, "Non-Photochemical Hole Burning in Tetracene-Doped Amorphous Anthracene," Chem. Phys. Lett. **95** (1983) 124.

Kishii, N., S. Tamura, N. Asai, K. Kawasumi, and J. Seto, "Photochemical hole burning of tetraphenylporphine derivatives," SPIE Proceedings (1989).

Kohler, W., J. Zollfrank, and J. Friedrich, "Stability of frequency domain information bits in amorphous organic materials," American Institute of Physics (1989) 3232.

Lee, H. W. H., M. Gehrtz, E. E. Marinero, and W. E. Moerner, "Two-color, photon-gated spectral hole-burning in an organic material," Chem. Phys. Lett. **118** (1985) 611.

Lee, H. W. H., and W. E. Moerner, "IBM Scientists Develop Novel High-Density Optical Storage Mechanism," Laser Focus/Electro Optics (1986) 24.

Lenth, W., R. M. Macfarlane, W. E. Moerner, F. M. Schellenberg, R. M. Shelby, and G. C. Bjorklund, "High-density frequency-domain optical recording," SPIE **695** (1986) 216.

Lenth, W., C. Ortiz, and G. C. Bjorklund, "Pulsed frequency-modulation spectroscopy as a means for fast absorption measurements," Opt. Lett. **6** (1981) 351.

Macfarlane, R. M., and R. M. Shelby, "Homogeneous line broadening of optical transitions of ions and molecules in glasses," J. Luminescence **36** (1987) 179.

Moerner, W. E., ed., *Persistent Spectral Hole-Burning: Science and Applications*, Springer-Verlag, New York (1988).

Moerner, W. E., M. Gehrtz, and A. L. Huston, "Measurement of Quantum Efficiencies for Persistent Spectral Hole Burning," American Chemical Society (1984) 6459.

Moerner, W. E., and M. D. Levenson, "Can single-photon processes provide useful materials for frequency-domain optical storage?" J. Opt. Soc. Am. B **2** (1985) 915.

Moerner, W. E., F. M. Schellenberg, and G. C. Bjorklund, "Photochemical Hole-Burning at GaAlAs Laser Wavelengths," Appl. Phys. B **28** (1982) 263.

Mossberg, T. W. "Time-domain frequency-selective optical data storage," Opt. Lett. **7** (1982) 77.

Mossberg, T. W., "Single shot stores bits," Technology Report **25** (1986) 36.

Mossberg, T. W., "Time-Domain Frequency-Selective Optical Memories," Proceedings 1989 LEOS Annual Meeting (Orlando, FL) 435.

Nishi, T., K. Arishima, H. Tabei, and H. Hiratuka, "Temperature Dependence of PHB Hole Profiles in Polymer Matrices," Jap. J. Appl. Phys. **27** (1988) 225.

Ortiz, C., R. M. Macfarlane, R. M. Shelby, W. Lenth, and G. C. Bjorklund, "Thin-Film Aggregate Color Centers as Media for Frequency Domain Optical Storage," Appl. Opt. **25** (1981) 87.

Pokrowsky, P., W. E. Moerner, F. Chu, and G. C. Bjorklund, "Reading and writing of photochemical holes using GaAlAs-diode lasers," Opt. Lett. **8** (1983) 260.

Rebane, A., "Associative space-and-time domain recall of picosecond light signals via photochemical hole burning holography," Elsevier Science Publishers B. V. **65** (1988) 175.

Rebane, A., and J. Aaviksoo, "Holographic interferometry of ultrafast transients by photochemical hole burning," Opt. Lett. **13** (1988) 993.

Rebane, K. K., R. K. Kaarli, P. M. Saari, and A. K. Rebane, "Time-and-space domain holography and optical information processing based on photoburning of spectral holes," SPIE Proceedings **963** (1988) 182.

Rebane, L. A., A. A. Gorokhovskii, and J. V. Kikas, "Low-Temperature Spectroscopy of Organic Molecules in Solids by Photochemical Hole Burning," Appl. Phys. B **29** (1982) 235.

Renn, A., S. E. Bucher, A. J. Meixner, E. C. Meister, and U. P. Wild, "Spectral hole burning: Electric field effect on resorufin, oxazine-4 and cresylviolet in polyvinylbutyral," J. Luminescence **39** (1988) 181.

Renn, A., A. J. Meixner, U. P. Wild, and F. A. Burkhalter, "Holographic Detection of Photochemical Holes," Chemical Physics **93** (1985) 157.

Renn, A., and U. P. Wild, "Spectral hole burning and hologram storage," Appl. Opt. **26** (1987) 4040.

Romagnoli, M., W. E. Moerner, F. M. Schellenberg, M. D. Levenson, and G. C. Bjorkland, "Beyond the bottleneck: submicrosecond hole burning in phthalocyanine," J. Opt. Soc. Am. **B1** (1984) 341.

Saari, P., R. Kaarli, and A. Rebane, "Picosecond time- and space-domain holography by photochemical hole burning," J. Opt. Soc. Am. **B3** (1986) 527.

Sakoda, K., K. Kominami and M. Iwamoto,"High Temperature Photochemical Hole Burning of Tetrasodium 5,10,15,20-tetra(4-sulfonatophenyl)porphin in Polyvinylalcohol," Japanese Journal of Applied Physics **27** (1988) L304.

Schmitt, U., and D. M. Burland, "Use of Holography to Investigate Photochemical Reactions from Higher Excited States. Action Spectrum of the Second-Photon Step in the Two-Photon Dissociation Reaction of Carbazole," J. Phys. Chem. **87** (1983) 720.

Shelby, R. M., R. M. Macfarlane, and D. P. Burum, "Optical Hole Burning and Coherent *rf* Double Resonance Spectroscopy of Rare Earth Ions in Solids," Appl. Phys. B **28** (1982) 262.

Tani, T., H. Namikawa, and K. Arai, "Photochemical hole-burning study of 1,4-dihydroxyanthraquinone doped in amorphous silica prepared by alcoholate method," J. Appl. Phys. **58** (1985) 355.

Thijssen, H. P. H., R. van den Berg and S. Volker, "Optical relaxation in organic disordered systems submitted to photochemical and non-photochemical hole-burning," Chem. Phys. Lett. **120** (1985) 503.

Thijssen, H. P. H., and S. Volker, "Pitfalls in the determination of optical homogeneous linewidths in amorphous systems by hole-burning influence of the structure of the host," Chem. Phys. Lett. **120** (1985) 496.

Thijssen, H. P. H., and S. Volker, "Spectral hole burning in semicrystalline polymers between 0.3 and 4.2 K," J. Chem. Phys **85** (1986) 785.

Tomlinson, W. J., E. A. Chandross, R. L. Fork, C. A. Pryde, and A. A. Lamola, "Reversable Photodimerization: a New Type of Photochromism," Appl. Opt.**11** (1972) 533.

Trommsdorff, H. P., J. M. Zeigler, and R. M. Hochstrasser, "Spectral hole burning in polysilanes," J. Chem. Phys. **89** (1988) 4440.

van den Berg, R., and S. Volker, "Does non-photochemical hole-burning reflect optical dephasing processes in amorphous materials? Pentacene in polymethylmethacrylate as an affirmative example," Chem. Phys. Lett. **127** (1986) 525.

Wild, U., Laser Focus/Electro-Optics (1987) 33.

Wild, U. P., S. E. Bucher, and F. A. Burkhalter, "Hole burning, Stark effect, and data storage," Appl. Opt. **24** (1985) 1526.

Winnaker, A., R. M. Shelby, and R. M. Macfarlane, "Photon-gated hole burning: a new mechanism using two-step photoionization," Opt. Lett. **10** (1985) 350.

Wu, W-Y, J. N. Schulman, T. Y. Hsu, and U. Efron, "Effect of size nonuniformity on the absorption spectrum of a semiconductor quantum dot system," Appl. Phys. Lett. **51** (1987) 710.

Yoshino, K., S. Nakajima, D. Park, and R. Sugimoto, "Spectral Change of Polymer Film Containing Poly(3-Alkylthiophene) with Temperature and Its Application as Optical Recording Media," Japanese Journal of Applied Physics **27** (1988) L454.